Drug delivery systems based on nucleic acid nanostructures

de Vries, Jan Willem; Zhang, Feng; Herrmann, Andreas

Published in:
Journal of Controlled Release

DOI:
10.1016/j.jconrel.2013.05.022

Publication date:
2013

Journal of Controlled Release 172 (2013) 467–483

Contents lists available at ScienceDirect

Journal of Controlled Release

journal homepage: www.elsevier.com/locate/jconrel

Drug delivery systems based on nucleic acid nanostructures

Jan Willem de Vries, Feng Zhang, Andreas Herrmann *

Department of Polymer Chemistry, Zernike Institute for Advanced Materials, University of Groningen, Nijenborgh 4, 9747 AG Groningen, The Netherlands

ARTICLE INFO

Article history:
Received 29 March 2013
Accepted 24 May 2013
Available online 3 June 2013

Keywords:
DNA
Nanoparticles
Nanotechnology
Drug delivery
Colloidal gold particles
DNA block copolymers

ABSTRACT

The field of DNA nanotechnology has progressed rapidly in recent years and hence a large variety of 1D-, 2D- and 3D DNA nanostructures with various sizes, geometries and shapes is readily accessible. DNA-based nanoobjects are fabricated by straight forward design and self-assembly processes allowing the exact positioning of functional moieties and the integration of other materials. At the same time some of these nanosystems are characterized by a low toxicity profile. As a consequence, the use of these architectures in a biomedical context has been explored. In this review the progress and possibilities of pristine nucleic acid nanostructures and DNA hybrid materials for drug delivery will be discussed. For the latter class of structures, a distinction is made between carriers with an inorganic core composed of gold or silica and amphiphilic DNA block copolymers that exhibit a soft hydrophobic interior.

1. Introduction

Since the discovery of the DNA double helix structure in 1953 many researchers have been intrigued not only by its role and the processes involved in storing genetic information but also by its utilization as a building block for nanostructures [1]. This trend has been fuelled by the introduction of automated solid phase synthesis, polymerase chain reaction and molecular cloning techniques allowing to produce oligonucleotides (ODNs) and long nucleic acid strands and make them available for a wide scientific community at an affordable price or effort. The versatile fabrication methods and the notion about the position of each atom within double-stranded (ds) DNA in combination with the unique self-recognition properties of DNA have made nucleic acids one of the most popular construction materials for nano-scale objects (Fig. 1) [2]. Early models of DNA self-assembly relied on the hybridization of single-stranded (ss) ODNs into double strands to form nucleic acid junctions [3,4]. Each junction is composed of four DNA sequences and contains short ss overhangs called "sticky ends" (Fig. 2A). These units provide a toehold for controlled assembly of multiple junctions, thereby creating a lattice of squares. In a similar way a cube can be formed by catenating six circular DNA strands mediated by hybridization and ligation (Fig. 2B) [5].

However, these assembly processes did not yield rigid junctions with defined angles and hence the geometry of the resulting structures was not well defined. To overcome these shortcomings two methods were developed to obtain well defined and structurally stable DNA nanoobjects. The first one involves DNA tiles that utilize the helical turn of DNA to form crossovers between two or more double strands within its structure (Fig. 3A). This design principle yields more rigid building blocks of high structural integrity that can be used for the construction of larger crystals of DNA [6,7]. Later this method was greatly expanded and generalized to allow the assembly of DNA into any desired shape like squares, triangles, star shapes or even smilies using a single viral DNA strand and many short ones that function as connecting elements, the "staple strands" [8]. An example of a 3D structure is a DNA box that contains a controllable lid (Fig. 1A) [9]. To date these DNA origami structures can be easily designed and synthesized and are applied for detection of biomolecules like proteins or DNA and for performing reactions at the nanometer scale [10–12].

The second method to obtain rigid DNA nanoobjects relies on the tensegrity principle (Fig. 3B) [13,14]. The squares considered earlier were unstable due to flexible junctions. DNA triangles, however, do not face this shortcoming and when the edges are composed of this motif rigid structures are obtained [15]. Therefore, many researchers have used this principle to construct a large number of DNA nanocages resistant to deformation like tetrahedra, octahedra, dodecahedra and icosahedra [16–20].

Aside from using pristine DNA as building block inorganic nanoparticles (NPs) have been used as template for the organization of ODNs. One very appealing template for this purpose is colloidal gold that was first used in 1996 when DNA functionalized gold nanoparticles (DNA-Au NPs) were introduced [21]. Thiol-terminated ODNs readily react with the surface of Au NPs and subsequent hybridization gives access to assemblies of higher order [22,23]. DNA-Au NPs offer some extra features like magnetic properties, plasmonic effects or the ability of fluorescence quenching, which represent a significant extension to the functionality of pristine DNA nanoobjects [24]. These characteristics are important in the field of bio-imaging

* Corresponding author.
E-mail address: a.herrmann@rug.nl (A. Herrmann).

0168-3659/$ – see front matter © 2013 Elsevier B.V. All rights reserved.
http://dx.doi.org/10.1016/j.jconrel.2013.05.022

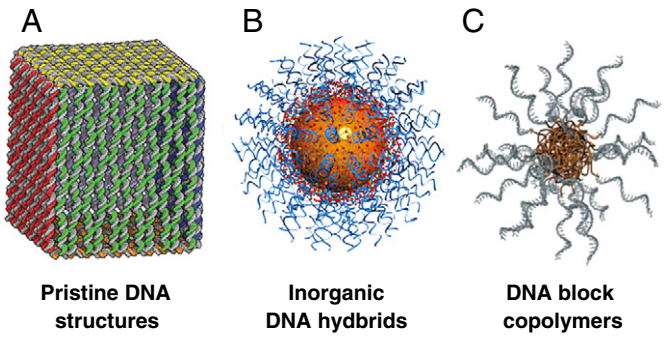

Fig. 1. Different classes of DNA nanostructures including (A) pristine DNA nanoobjects, (B) inorganic-DNA hybrid materials and C) assemblies of amphiphilic DNA block copolymers. Reproduced with permission from [9,24].

and biomedicine; hence DNA-Au NPs have become a very popular template for the assembly of nanoobjects and currently find use in imaging, detection and as transfection agents and gene regulation materials [25–28].

In addition to DNA nanoparticles with an inorganic core such structures can be produced with a soft interior. The realization of these structures implies the use of synthetic organic polymers. The first DNA polymer conjugates date back to the late 1980s, where poly(L-lysine)-*block*-DNA was used as anti-viral agent [29,30]. Nowadays, nucleic acid-polymer hybrid materials are already in clinical use [31]. Thereby, a hydrophilic synthetic macromolecule component was connected to an aptamer for increasing the in-vivo stability of the nucleic acid. For the realization of DNA polymer nanoobjects hydrophobic polymers need to be attached to the DNA units to achieve self-assembly into larger aggregates. The first example of such an amphiphilic biodegradable DNA block copolymer (DBC) contained poly(D,L-lactic-*co*-glycolic acid) as a hydrophobic polymer block [32]. These compounds form micellar structures that exhibit a hydrophobic core and a hydrophilic corona of ss DNA. More recently, several groups realized such micellar morphologies and in addition showed that the overall structure can be altered from spherical to cylindrical assemblies by stimuli like changes in pH, addition of endonucleases or through hybridization with complementary DNA [33,34]. Due to these unique properties, DBCs are currently applied in purification of biomaterials [35,36], DNA detection [37], templated synthesis [38] and in nanoelectronics [39].

All classes of DNA nanomaterials described above have in common that the size and shape are very well defined, probably better than in any other bottom-up fabricated material. This feature has dramatic consequences for applications in the field of biomedicine where multifunctional nanoparticles start to play an increasingly important role, especially in the areas of drug delivery and bioimaging. The DNA nanoobjects act as a shape persistent scaffold allowing precise positioning of various moieties like targeting units or drug payloads.

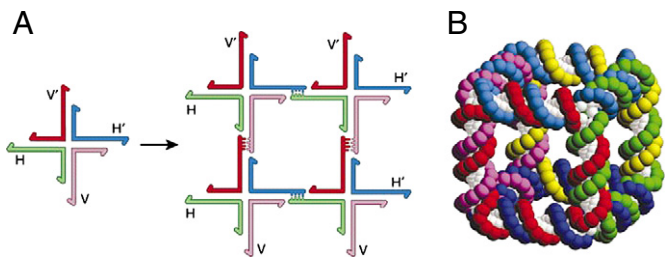

Fig. 2. (A) On the left a representation of a nucleic acid junction formed from four ss DNA sequences is shown and on the right the corresponding lattice formed by hybridization of the sticky ends is depicted. (B) DNA cube formed by catenated circular DNA strands.
Reproduced with permission from [4].

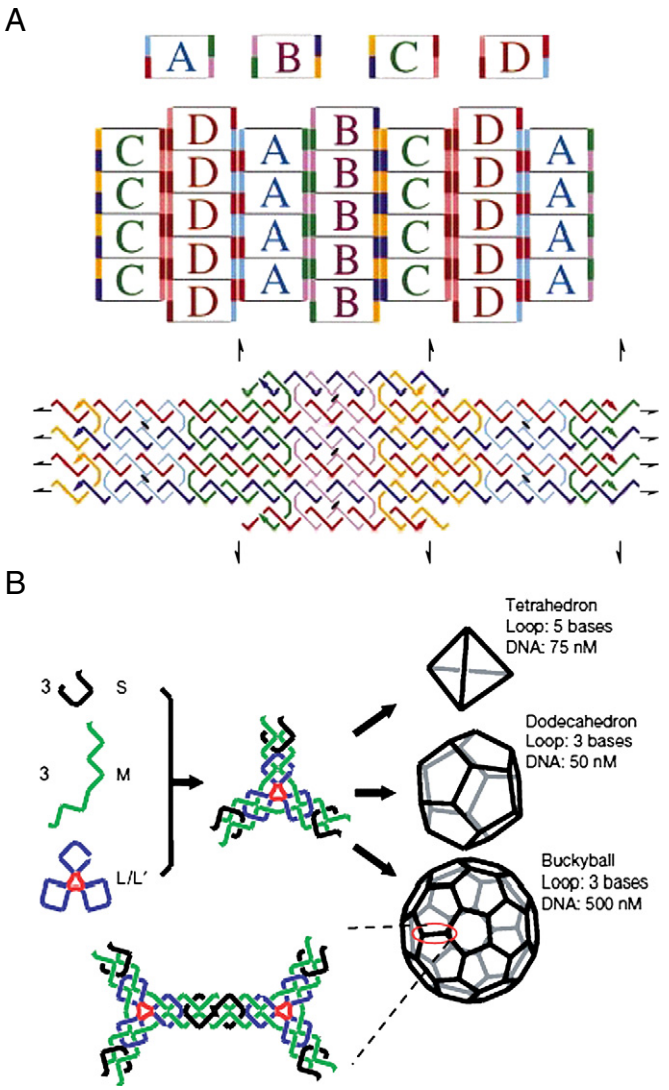

Fig. 3. Assemblies based on DNA tiles. (A) A 2D-pattern of DNA that is based on four different tiles named A, B, C and D. The colors at the vertical edges represent overhangs that hybridize with overhangs of other tiles with the same color (top). Example of a single DNA tile (bottom). (B) DNA tiles that self-assemble into 3D-nanoobjects. Reproduced with permission from [6,20].

On the other hand all the different types of DNA assemblies exhibit distinctive properties. While the functionality of a pristine DNA scaffold is relatively limited, in the case of DNA hybrid materials extra functions are implemented via the non-nucleic acid components. All these different features will be highlighted in this review article.

Although the use of DNA nanoobjects in biomedicine is still in its early stages, promising examples have been provided that demonstrate the applicability and benefits of using DNA-based nanomaterials over other systems like liposomes, polymeric micelles and polymersomes [40–43]. The most obvious use of oligonucleotide nanostructures in the medical field is the delivery of siRNA, antisense RNA or genes. However, several excellent reviews on this topic have been published recently [44–47]. The same holds true for DNA nanoobjects employed in the context of cellular and in-vivo bioimaging [48,49]. Therefore, both topics will not be covered in this manuscript. Here we will summarize the use of pristine DNA nanoobjects and DNA hybrid materials as carriers in the field of therapeutic delivery and vaccination. For the different classes of DNA nanomaterials we start with describing the preparation methods followed by the stability in biological

environments and cell uptake behavior. Finally, we discuss controlled release or performance of the nanostructures in-vitro and in-vivo.

2. Delivery with pristine DNA scaffolds

2.1. DNA tetrahedra

While the field of DNA nanotechnology aimed for increasing the structural complexity, which is often associated to the utilization of a large number of DNA strands per nanoobject, the demands for DNA-based carrier systems pose different requirements on the design. Since for in-vitro and in-vivo experiments usually larger quantities of materials are needed, the number of strands per DNA nanostructure with different sequence composition should be kept at a minimum due to cost issues. For the same reason the lengths of the sequences should be limited. One example of such a structure consisting of a small number of sequences is the DNA tetrahedron [50] and it was even demonstrated that this nanoobject can be prepared from a single DNA strand of 286 nucleotides (nt) [16]. While this approach requires the synthesis of DNA by rolling circle amplification or in-vivo replication, the same object can be realized from four chemically synthesized single strands of 55 nt. The resulting structures exhibit edges being composed of 17 base pairs (bp) of ds DNA which equals 5.8 nm considering a length of 0.34 nm per bp (Fig. 4, top) [50]. An object of the same geometry was realized by assembly of DNA tiles [51]. Seven strands were converted into a tile and four of these units form a tetrahedral structure. At the middle of each strut of the tetrahedron one ss overhang was incorporated that allows the implementation of a triangular feature within each plane of the object (Fig. 4, bottom). By the addition of interfering strands these inserts can be removed allowing the change of porosity of the tetrahedron's surface, which might be important for the trapping and release of cargo.

Initial experiments for the cell uptake of a tetrahedral DNA nanostructure were performed without any cargo [52]. For that purpose cultured human embryonic kidney cells were incubated with fluorescently labeled DNA cages. The uptake was investigated by confocal microscopy and flow cytometry. Significant internalization of the tetrahedron was detected for pristine nanoobjects and for ones treated with a transfection reagent. Subcellular localization revealed presence of the cages in the cytosol. Stability experiments were carried out employing Förster resonance energy transfer (FRET) experiments indicating structural integrity of the DNA cages for at least 48 h. The same cages were equipped with CpG motifs to induce immunostimulation [53]. CpG motifs are short oligonucleotides where a 2′-deoxycytidine is connected by a phosphodiester bond to 2′-deoxyguanosine. When these nucleotides are unmethylated as in natural viral and bacterial DNA they have immunostimulatory activity [54]. This CpG motif occurs very rarely in vertebrate genomes and is therefore considered a pathogen-associated molecular pattern indicating invasion of pathogens [55]. In this context the first step of eliciting an immune response is binding of CPG ODNs to Toll-like receptor 9 (TLR9) present in B cells and plasmacytoid dendritic cells (pDCs), which is followed by a signaling cascade [56]. In a therapeutic context, CpG ODNs can be applied as an agonist of TLR9 to boost the immune response which is favorable during the treatment of cancer and allergic diseases [57]. For that reason CpG-derived ODNs were investigated and tested in preclinical studies as vaccine adjuvants [58,59].

When the CpG motifs were appended to the tetrahedron, the nanoobjects were resistant to nuclease degradation and remained intact in fetal bovine serum and in cells for at least several hours. More important, they entered macrophage-like RAW264.7 cells without transfection agents and their CpG motif was recognized by TLR9. As a result of that binding event immunoregulatory downstream pathways were activated (Fig. 5, top). Various pro-inflammatory cytokines including tumor necrosis factor (TNF)-α, interleukin (IL)-6 and IL-12 were up-regulated. Due to the fact that the tetrahedral nanostructures are mechanically stable several CPG motifs attached to the surfaces were accessible for TLR9 which resulted in a multivalency effect of enhanced immunostimulation (Fig. 5, bottom) [60].

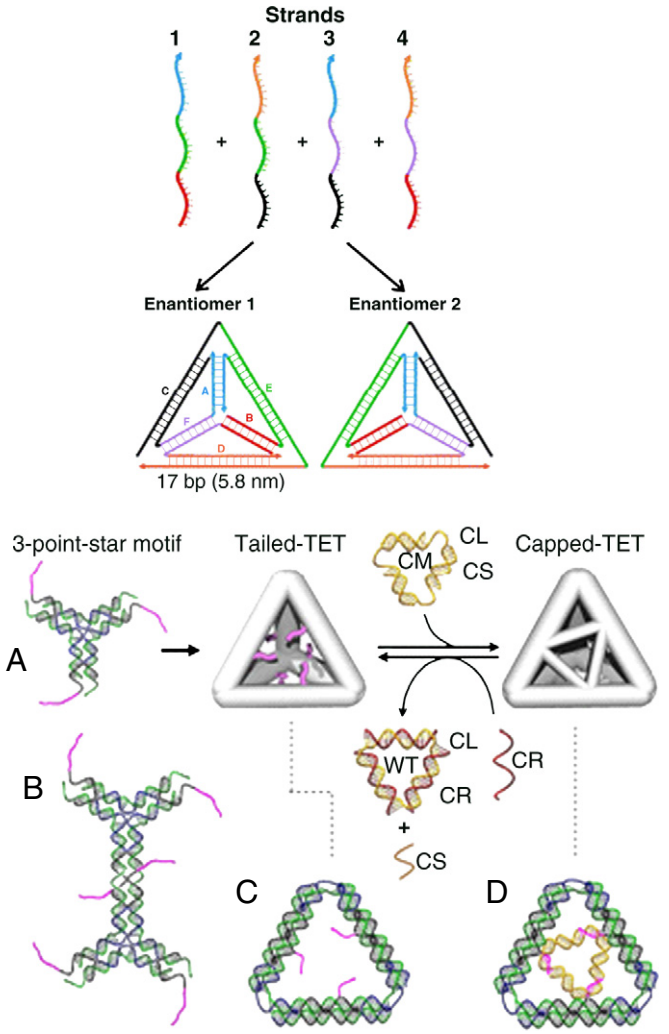

Fig. 4. (top) Synthetic scheme for a tetrahedron composed of four DNA strands. (bottom) Schematic design of the DNA tetrahedron with controllable porosity. (A) Four 3-point-star tiles are used to construct a DNA tetrahedron with extended ss tails near the middle of the struts, offering the binding sites for the capping motif (CM), which is formed through hybridization of a longer circular DNA strand (CL) with three copies of shorter strands (CS). CM can be removed by addition of a cap-removal strand (CR) that is fully complementary to CL. (B) Details of dimer formation between two 3-point-star motifs. (C, D) Face structures of a uncapped and capped tetrahedron, respectively.
Reproduced with permission from [50,51].

After these successful in-vitro experiments DNA tetrahedra equipped with CpG motifs were employed in-vivo for vaccination (Fig. 6A) [61]. Therefore, streptavidin (STV) was incorporated into the DNA nanocages to form an antigen–adjuvant complex. The immunogenicity of this complex was assessed in a BALB/c mouse model by measuring the anti-STV antibody response and comparing it to an unassembled mixture of STV and CpG ODN or STV alone. It was found that mice immunized with the STV-CpG ODN-tetrahedron developed a much higher level of anti-STV IgGs than the above mentioned controls after a period of 70 days. To substantiate this outcome antibody secreting cells (ASCs) that originate from STV-specific memory B cells present in spleen cells were quantified (Fig. 6B). Significantly elevated levels of specific ASCs were determined for mice immunized with the tetrahedron-CpG ODN–STV complexes compared to those immunized with free CpG + STV and STV only. These results indicate that the fully loaded tetrahedron induces a strong and long-term immunity against the antigen due in part

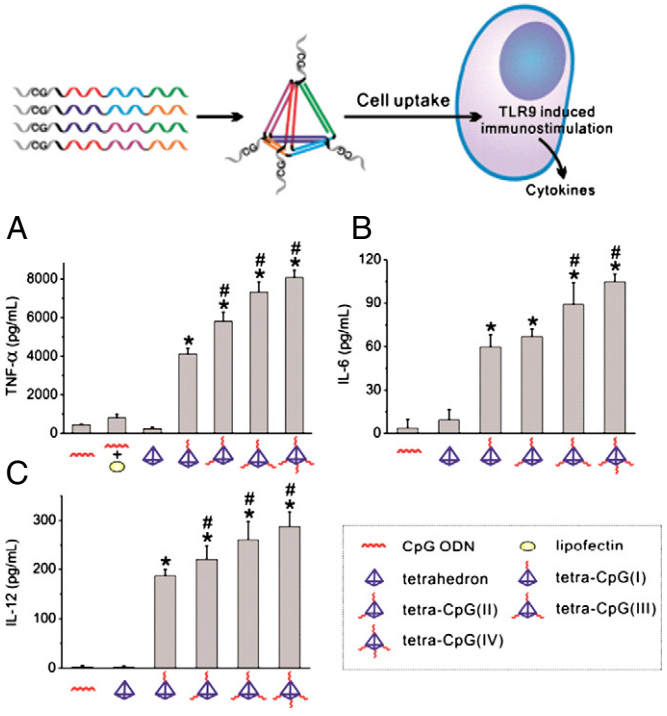

Fig. 5. (top) Assembly of CpG grafted DNA tetrahedron delivery systems for eliciting an immune response. (bottom) Release levels of cytokines TNF-α (A), IL-6 (B) and IL-12 (C) from RAW264.7 cells using different immunostimulatory nanoobjects.
Reproduced with permission from [60].

to the generation of STV-specific memory B cells. Further experiments proved the safety of the DNA carrier because no immune response against the carrier, i.e. a ds DNA tetrahedron, was developed, which could result in tissue damage or trigger autoimmunity [61]. This work shows the great potential of scaffolds generated by DNA nanotechnology to serve as a general platform for vaccine development. A major part of the DNA tetrahedron's potency in the biomedical field is derived from its rigid 3D scaffold allowing specific multivalent interactions with cellular components.

However, DNA tetrahedra with a flexible unit were generated as well [62]. One of the struts of the tetrahedron was constructed from a ss RNA aptamer recognizing ATP. When this assembly was internalized into HeLa cells ATP levels within living cells could be measured indicating that the construction of intracellular logic sensors is feasible.

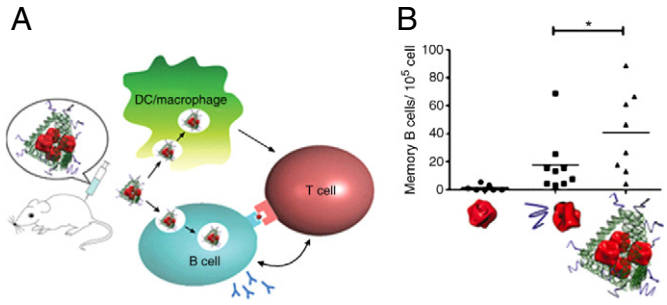

Fig. 6. (A) Schematic drawing of the DNA tetrahedron vaccine complex containing the antigen streptavidin (red) and CpG ODNs (purple). (B) ELISPOT assay of specific memory B cell response in mice stimulated by STV, STV + CpG and CpG-STV DNA tetrahedron, respectively.
Reproduced with permission from [61].

2.2. Branched DNA nanostructures and polypods

The DNA tetrahedron represents a simple shape persistent scaffold allowing to present four units at each vertex like the CpG motif or cell surface recognizing aptamers. Equally simple regarding the design but of more structural flexibility are branched structures or polypods. The simplest assembly of this type is Y-shaped and can be constructed from three ODN strands (Fig. 7, top) [63]. Already in 2008 such a DNA nanostructure was equipped with several immunostimulatory CpG motifs [64]. Cytokine production (TNF-α and IL-6) after addition of the Y-structure to RAW264.7 cells was measured. It was found that the ds Y-shape is effective in inducing greater amounts

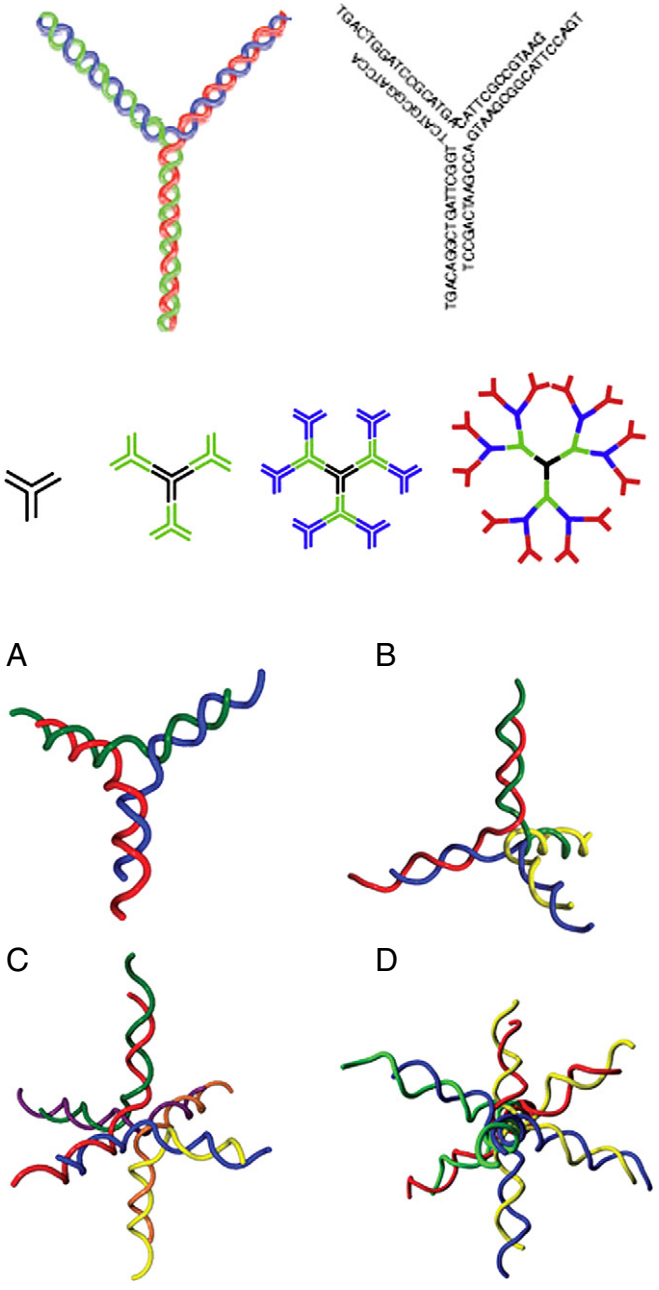

Fig. 7. (top) Schematic representation of Y shaped ODNs. (middle) Schematic design of dendrimer-like DNA (DL-DNA), from left to right: Y-DNA; first generation DL-DNA, second generation DL-DNA, and third generation DL-DNA, (bottom) Schematic representation of models of polypods: (A) tripod-DNA, (B) tetrapod-DNA, (C) hexapod-DNA and (D) octapod-DNA.
Reproduced with permission from [63,65,66].

of TNF-α and IL-6 in macrophage like TLR9-positive cells than conventional ss or ds ODNs containing the same amounts of CpG motifs. This high immunostimulatory activity of Y-ODN is at least partly associated with increased uptake by the TLR9-positive cells but not with stabilization through the DNA nanostructure. Other factors like higher affinity of Y-ODN to the TLR9 receptor or intracellular localization may also contribute to the increased immunostimulation.

In a follow up study the same authors fabricated dendritic DNA nanostructures by ligating Y-shaped DNA monomers [65]. In this manner, the second and third dendrimer generation were fabricated with 12 and 24 CpG motifs located at the periphery of the DNA nanostructures, respectively (Fig. 7, middle). The dendritic DNA architectures induced greater amounts of TNF-α and IL-6 from RAW264.7 cells than a mixture of Y-shaped DNA encoding the same CPG motifs as present in the dendrimers. The dendritic DNA was internalized six to 15 times more efficiently by the macrophage-like cells than Y-DNA, which resulted in the secretion of much greater (100-fold or more) amounts of cytokines. These results suggest that a dendritic architecture with multiple CpG motifs at the rim is a viable design for a DNA nanostructure to increase the immunostimulatory activity without any chemical modification of the natural phosphodiester DNA backbone.

In addition to the trigonal Y-shaped unit, polypods with a higher degree of branching were evaluated regarding their immunostimulatory potential [66]. For that purpose a tri-, tetra-, hexa- and octapod consisting of three, four, six and eight ODNs, respectively, were assembled (Fig. 7, bottom). Again at the end of the branches CpG motifs were established yielding assemblies consisting of DNA in the B-form with a diameter of around 10 nm. The melting temperature of the nanoobjects decreased with increasing the degree of branching. Each polypod DNA induced the secretion of TNF-α and IL-6 from macrophage-like RAW264.7 cells to a greater extent than ss or ds non-branched CpG containing DNA. Evenly important, the highly branched architectures, i.e. hexa- and octapod, were more effective in stimulating cytokine production than the structures with a lower branching degree, i.e. tri- and tetrapod. Other properties that are dependent on the degree of branching are the uptake and the stability in serum. The more branched the polypods are the better they are taken up in TLR9-positive cells but the less stable they are. From these results it could be concluded that the CpG-containing polypods with hexagonal and octagonal symmetry are promising biodegradable nanoobjects with high immunostimulatory activity.

2.3. DNA icosahedra

In addition to directly using branched DNA structures for immunostimulation, more complex polyhedra can be fabricated from those building blocks. The resulting assemblies contain a triangular tensegrity motif and were employed for drug delivery purposes [67]. From six individual DNA single strands, six-point-star motifs were formed (Fig. 8A) that via sticky end cohesion self-assemble into an icosahedron (Fig. 8B). In one of the six strands an aptamer sequence was incorporated that protrudes from the icosahedron surface and is responsible for MUC 1 recognition. This protein belongs to an important class of tumor surface markers which are uniquely expressed on a broad range of epithelial cancer cells with high abundance [68,69]. The final step of the carrier fabrication consisted of loading of doxorubicin (Dox) by intercalation (Fig. 8C). This anthracycline derivative is frequently employed in chemotherapeutic anticancer treatment [70–72]. The potency of the icosahedral carrier system was assessed by in-vitro cell culture experiments employing flow cytometry, confocal fluorescence microscopy and cytotoxicity tests. In co-culture experiments it could be demonstrated that the DNA nanocarrier was efficiently taken up by the human breast cancer cell line MCF-7 that is MUC1 positive while no internalization was observed in Chinese hamster ovary cells (CHO-K1) that do not express MUC1. Besides this superb targeting function the Dox-loaded carrier exhibited a greater cytotoxicity in MCF-7 cells than free Dox indicating specific and efficient delivery of anticancer drugs and suggesting the potential use of DNA icosahedra for use in targeted cancer therapy [67].

Another function that was realized with icosahedral DNA nanostructures is in-vivo imaging [73]. Therefore, fluorescein isothiocyanate (FITC)-labeled dextran (FD10) with a molecular weight of 10 kDa was encapsulated in an icosahedral DNA cage. The encapsulation procedure starts with the formation of two icosahedral halves from five-way junctions similar as described above (Fig. 9A) [19]. These two assemblies were incubated with FD10 and subsequently joined by hybridization resulting in a full DNA icosahedron containing two FD10 units within their interior (Fig. 9B). These host guest complexes were microinjected into *Caenorhabditis elegans*. This organism is a nematode that contains scavenger cells, called coelomocytes, which endocytose fluid from the pseudocoleom. After introducing the loaded icosahedra these nanoobjects were specifically internalized by the coelomocytes due to interactions with anionic ligand-binding receptors and subsequent receptor-mediated endocytosis. In stark contrast, the pristine FD10 lacks negative surface charges and was therefore taken up by fluid phase endocytosis resulting in its non-specific distribution throughout the pseudocoleom after microinjection. After proving the complete alteration of endocytotic uptake pathways due to different molecular interactions the functionality of the cargo was examined

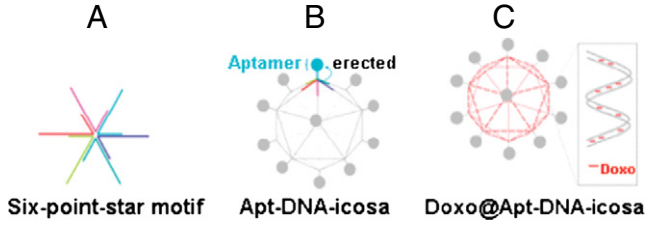

Fig. 8. Schematic representation of (A) the six-point-star motif, (B) the DNA icosahedron and (C) the DNA icosahedron containing intercalated Dox for targeted delivery. Reproduced with permission from [67].

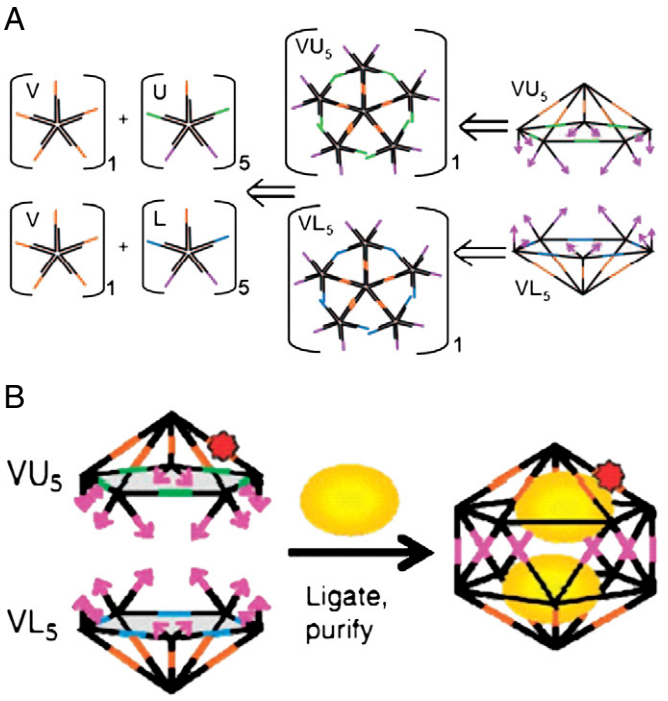

Fig. 9. (A) Synthetic strategy for constructing the DNA icosahedron, (B) encapsulation of (FITC)-dextran into DNA icosahedron.
Reproduced with permission from [73].

in-vivo. Due to their pH sensitivity, FITC on Dextran was employed as pH sensor to measure the proton concentration in organelles, inside cells and whole organisms [74,75]. When encapsulated in the DNA nanocage this function remains unchanged and the host guest complexes were employed to map the pH changes during endosomal maturation along the ALBR pathway in coelomocytes in living worms. This work represented the first demonstration of functionality and emergent behavior of a cargo-loaded DNA nanostructure in-vivo [73].

2.4. DNA origami

As introduced above, the DNA origami technique deals with folding a ss long DNA strand into almost any 2D or 3D shape with the help of many different "staple" strands [8,76]. These strands bind to the long one at different positions to define the overall structure and they can be utilized to site specifically introduce additional functionalities by hybridization.

Before the DNA origami structures were introduced for biomedical purposes their stability in cell lysates was investigated [77]. Four assemblies were fabricated for that purpose: a 2D rectangular origami (90 × 60 nm) [10], a 2D equilateral triangle (120 nm long with 30 nm wide sides) with an open central triangular cavity of 60 nm per side, a 3D multilayer rectangular parallelepiped structure (16 × 16 × 30 nm) and a 2D rectangular structure with staple strands bearing overhangs allowing hybridization (Fig. 10A) [10]. These DNA architectures were incubated with cell lysate from which nuclear DNA and cell membrane debris were removed. After incubation times of 1 and 12 h the origami structures were investigated by non-denaturing gel electrophoresis and by direct visualization employing AFM as well as transmission electron microscopy. Taking into account all three methods it can be concluded that all the origami assemblies are stable at 25 °C with the cell lysates tested, i.e. metaplastic human esophageal epithelial cell line [78], End1/E6E7 cells, MCF-10A cells and cancerous HeLa and MDA-MB-231 cells. In contrast, ss M13mp18 viral DNA and ds λ DNA that acted as control showed alterations already after 1 h incubation with the cell lysates. Finally, it was demonstrated that ss DNA features protruding from the origami structures remained intact and could be successfully used for detection of mRNA from the lysate (Fig. 10B). These results suggest that DNA origami scaffolds have the potential to serve as an in-vitro diagnostic platform and might be of importance for single cell proteomic analysis when integrated into microfluidic chips.

The same results also confirm the stability of DNA origami objects inside cellular environments and therefore their application as delivery vehicle will be discussed in the following paragraph. As shown above many DNA nanostructures were tested regarding their immunostimulatory potency when equipped with CpG motifs. For the same purpose structurally complex DNA origami scaffolds were successfully utilized as well. Freshly isolated spleen cells were incubated with a hollow 30-helix origami tube (approximately 80 × 20 nm) with 62 binding sites for hybridization of CpG motifs distributed over the surface. This DNA origami scaffold that was constructed from M13mp18 DNA (8634 nt) and 227 staple ODNs was taken up into endosomes and triggered a strong immune response indicated by cytokine secretion, which was entirely dependent on TLR9 stimulation. As controls for the DNA origami tubes, CpG ODNs complexed with lipofectamine, a standard transfection agent, were employed which showed lower immunostimulation when applied at equal amounts. Tubes without hybridized CpG motifs induced a low amount of cytokine production that was not related to TLR9 recognition. In contrast to the cationic carrier lipofectamine, the DNA tubes exhibited no detectable cytotoxicity for splenocytes and therefore qualify themselves as an efficient and non-toxic immunostimulants.

Similar tubes as generated for immunostimulation were harnessed for cancer therapy [79]. In this study two types of DNA origami tubes were employed that were smaller than the one applied for immunostimulation. The first type exhibited a straight nanotube structure

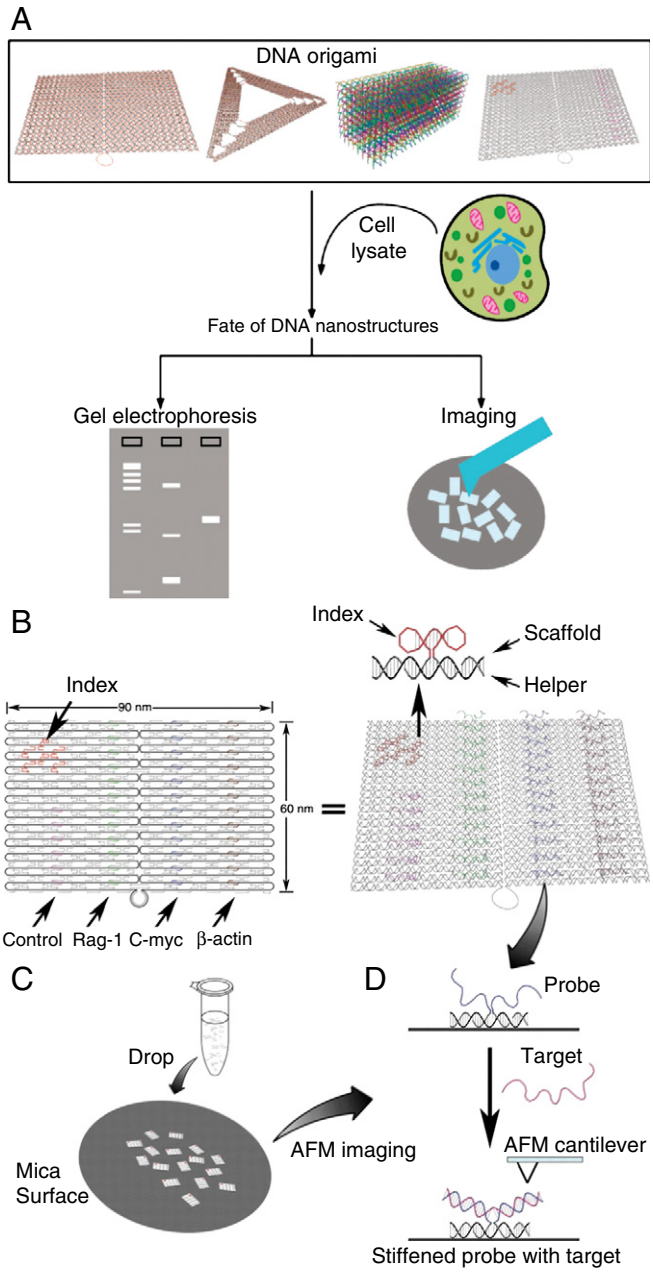

Fig. 10. (A) DNA origami structures used for testing the stability in cell lysate, from left to right: 2D rectangle, 2D equilateral triangle, 3D multilayer rectangular structure and a 2D rectangle with staple strands bearing ss overhangs. (B) (Left) Schematic representation of DNA origami structure for nucleic acid detection (Rag-1, C-myc, β-actin and control). The DNA square was composed of circular single-stranded M13 viral DNA (black) and >200 staple strands. Through incorporation of helper strands ss overhangs were formed allowing for hybridization with the target sequence. (Right) 3D illustration of the DNA origami. (C) Representation of target detection using DNA origami structures. (D) (Top) ss helper strands on top of the tile and (bottom) detection of target sequence using atomic force microscopy (AFM).
Reproduced with permission from [77] and [10].

using a conventional number of 10.5 bases per helical turn to determine crossover positions between neighboring helices. This S-Nano design relied on a scaffold strand containing 7560 nt, exhibited a length of 138 nm and a diameter of 13 nm. As a second design, a twisted version (called T-Nano) with similar dimensions was constructed (Fig. 11). It is based on an 8634 nt long scaffold and during hybridization of staples every seventh nt an insertion was introduced similar as reported before [80]. The accommodation of 12 bp per turn resulted in a global right handed twist to partially relief the stress induced by imposing an

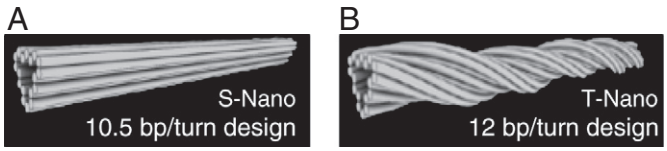

Fig. 11. 3D models of (A) straight nanotube (S-Nano), using 10.5 bp per turn twist density and (B) twisted nanotube (T-Nano), having 12 bp/turn.
Reproduced with permission from [79].

unnatural twist density on the DNA. Subsequently, an anticancer drug was loaded into the DNA origami tubes by intercalation. The T-Nano design was able to accommodate 33% more Dox than the S-Nano structure although T-Nano contains only 14% more base pairs than the straight tube. The difference in loading capacity might be explained by the higher affinity of Dox to the 12 bp/turn helix. After loading, the release from the tubes was studied. The T-Nano design retains the drug to a larger extend than S-Nano resulting in a slower release profile. The release kinetics of T-Nano indicated that 50% of the drug could be retained for more than several hours which was translated into a higher toxicity of this system towards three different breast cancer cell lines (MDA-MB-231, MDA-MB-468 and MCF-7) compared to free Dox. The S-Nano/Dox system and ds DNA loaded with Dox were less potent in similar experiments. These findings and the non-toxic nature of the T-Nano origami structure itself suggest that twisted DNA origami designs are a suitable delivery platform for targeted cancer therapy.

In a different study it could even been shown that DNA origami carriers have the potential to overcome drug resistance [81]. A DNA origami tube and a triangle were loaded with Dox, similar as described above, and were administered to drug sensitive (reg) and drug resistant (res) MCF7 human breast adenocarcinoma cells (Fig. 12). Free Dox and Dox-loaded origami assemblies were both active in killing the reg-MCF7 cell line. In contrast, free Dox and ds DNA with intercalated Dox moieties were not effective in inducing cell death in res-MCF7 cells. However, when the same cells were incubated with the origami structures containing the same amount of Dox as the above controls cell death was induced. This is a strong hint that DNA origami structures have the potential to overcome Dox resistance. In the next step the reason for this characteristic of the origami carrier was investigated. The origins of cultured cancer cells becoming resistant against cytotoxic anticancer drugs can be manifold [82,83]. One of the most common reasons is decreased drug concentrations inside the cells as e.g. induced by efflux pumps in the membrane that eject drugs or decrease drug uptake. In this regard, it was demonstrated that the folded DNA nanostructures increase the uptake of the anticancer drug in res-MCF7 cells. Another reason for the development of multidrug resistance is related to intracellular pH, both in the cytoplasm and in acidic organelles [84]. In tumor cells with a resistant phenotype the anticancer drugs are predominantly localized in acidic compartments like the lysosomes and are therefore not able to reach the site of action, i.e. the cytosol or nucleus [85]. Therefore, the co-administration of agents liberating the drugs from these compartments was carried out allowing redistribution of the drug to the active sites [86,87]. In this study, it was revealed that treatment of res-MCF7 cells with Dox-loaded origami objects resulted in elevated pH indicating the inhibition of acidification of lysosomal compartments. Taken together, overcoming drug resistance by the origami assemblies can be explained by a combination of two features. Firstly, the origami scaffold increases Dox uptake and, secondly, induces a change of pH in lysosomes leading to a redistribution of the drug to the target sites.

A more complex vehicle regarding functionality was based on an origami design consisting of a hexagonal barrel with dimensions of 35 nm × 35 nm × 45 nm (Fig. 13) [88]. This called logic-gated nanorobot was constructed in such a way that the two domains forming the barrel were covalently connected at the rear and were non-covalently fastened twice at the opposite site. These two non-covalent connections were designed as DNA aptamer-based locks that open in response to antigen keys. In the closed state the lock consists of an aptamer–complement duplex that after binding of the molecular "key" dissociates or opens to form an aptamer–target complex. Due to the presence of two aptamer locks at the front side a logic gate-type behavior can be implemented into the origami structure. When the locks are equipped with sequences recognizing different targets opening of the barrel only occurs when both antigen keys are present emulating an AND-gate behavior. Inside the DNA barrel 12 attachment sites were placed for the incorporation of cargo molecules by hybridization. Au nanoparticles and Fab antibody fragments covalently connected to ODNs served as payload. After locking and loading the functionality of the nanorobot was tested. It was demonstrated that when the proper combination of antigen keys was present the nanorobot opens its barrel structure and binds to a cell surface which was measured by flow cytometry due to the presence of a fluorescent label that was attached to the payload antibodies. Finally, the nanorobots were investigated in regard to their ability to get activated and interfaced to cells to interfere with signaling pathways. Thereby it was demonstrated that after specific unlocking the nanorobots induced growth arrest in leukemic cells in a dose

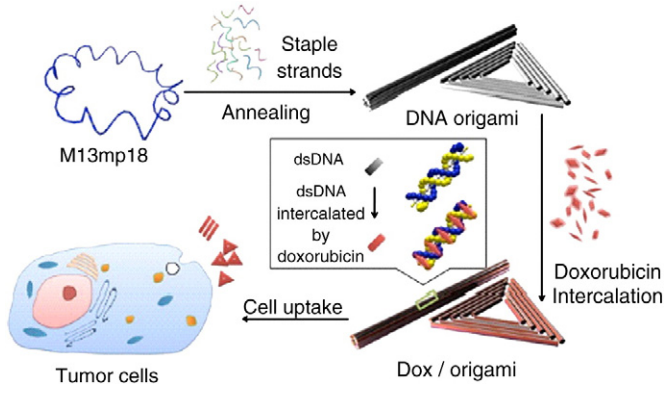

Fig. 12. Schematic representation of DNA origami systems, DNA tube and DNA triangle, for Dox delivery.
Reproduced with permission from [81].

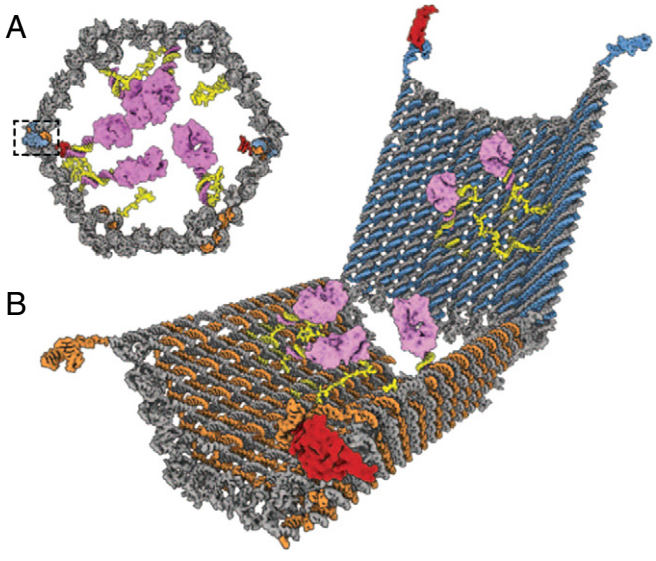

Fig. 13. (A) Schematic front orthographic view of DNA nanorobot in the closed state with a protein payload attached inside. (B) 3D view of DNA nanorobot in the open state.
Reproduced with permission from [88].

dependent manner. In addition to the inhibition task, various methods of signaling pathway activation were demonstrated. It was shown that nanorobots could collect flagellin from solution and induce T cell activation. All the experiments prove that the origami robots can induce a variety of tunable changes in cell behavior. Moreover, bioactive molecules may be introduced indirectly via interactions with loaded antibody fragments, enabling applications in which the robot fulfills a scavenging task before targeted payload delivery.

While all the origami structures in this paragraph consist of many different units, especially a high number of staple strands, efforts to reduce the quantity of building blocks are necessary for costs efficiency and practical applications. One such alternative to the origami method to produce tube structures is the utilization of rolling circle amplification (RCA). RCA is an enzymatic method that allows the fabrication of long, ss DNA of periodic sequence from cyclic templates. The resulting RCA products were employed to construct long tracks of proteins [89] and nanoparticles [90]. For the assembly of nanotubes, a circular ss DNA was combined with a primer strand and DNA polymerase Phi29 producing the periodic ss DNA **Guide** (Fig. 14) [91]. This long DNA strand coding alternatingly binding regions (**BR**) and spacer regions (**SR**) was hybridized with spacer strand **1a** to form **1**. The ss BR was then hybridized with triangular rung **2** to result in an open nanotube **RCA-NT$_o$**. This extended structure was transformed in the closed tube **RCA-NT**. The dimensions of such triangular tubes could be controlled by the length of the RCA product ranging from around 0.7 to 1.2 μm. Similar as the origami tubes, the RCA-derived assemblies were more resistant towards the digest by nucleases compared to conventional ds DNA and they were internalized in human cervical cancer cells (HeLa). With the same cell line, uptake of ds DNA was negligible. Combined with their proven uptake and release behavior these DNA-economic nanotubes are a potentially unique platform for drug delivery and bioimaging [92].

An even more reductionist approach regarding sequence efficiency is the use of a single DNA strand that governs the ability to self-assemble into a tube [93]. This 52 nt long strand is divided into four segments which exhibit a length of 10, 16, 16 and 10 bases, respectively, and are all self-complementary. Due to that particular design they assemble into tubes with a length of up to 60 μm and varying diameters in the range of several tenths of nanometers. Initial steps towards employing these DNA tubes for targeted cancer therapy have been undertaken. The 52 nt DNA strands were conjugated to folic acid, a targeting unit, and Cy3, a fluorescence imaging agent. Subsequently, cancerous KB cells that overexpress the folate receptor were incubated with the dually labeled nanotubes. The 1D nanostructures were strongly adsorbed on the cell surface and parts of them effectively internalized. At the same time, like for other DNA tube constructs, they showed no obvious toxicity.

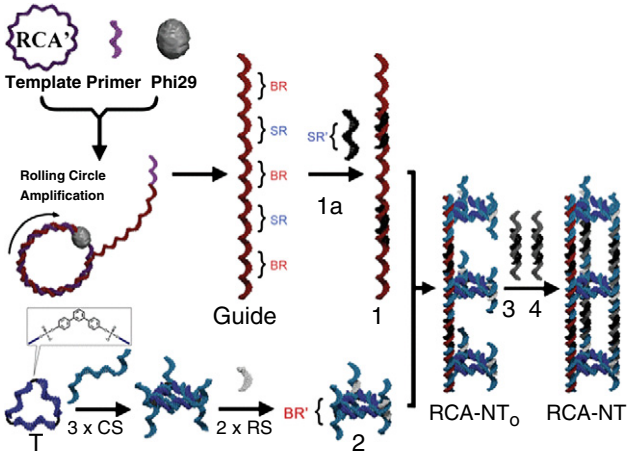

Fig. 14. Design of RCA nanotubes. The backbone strand **1** with alternating segments of **BR** and **SR** is prepared by RCA. On each vertex of triangular rung **2**, two well oriented ss DNA sequences extend longitudinally for hybridization with **1** to construct the open nanotube **RCA-NT$_o$**. Double-stranded linkers **3** and **4** are used to form the full nanotube **RCA-NT**.
Reproduced with permission from [91].

3. Delivery with scaffolds consisting of nucleic acids combined with other materials

There are several differences between the DNA nanostructures described above and the hybrid materials discussed in this paragraph. The dominant motif in all pristine nucleic acid assemblies is the DNA double helix forming a rigid and to a great extent shape persistent scaffold. In DNA nanostructures derived from DNA hybrid materials both single- and double-stranded nucleic acids are found. In those materials the orientation of the DNA is dictated by the attachment to the core not by hybridization. While pristine DNA assemblies almost exclusively rely on Watson–Crick base pairing, nanostructures from DNA hybrid materials are formed by covalent bonds either to an inorganic core or to a hydrophobic polymer. Various core structures are known that served as anchoring points like Au [94], Ag [95], Fe_3O_4 [96], CdSe [97], or hydrophobic polymers [98–100].

3.1. DNA nanoparticles with an inorganic core

3.1.1. DNA-Au NPs

The most important inorganic core material in the context of drug delivery is Au. DNA-Au NPs were fabricated by mixing ODNs containing a terminal sulfhydryl group with citrate-stabilized colloidal Au NPs. The ODNs replace the small ligand and cover the surface [21]. To increase the density of DNA a method called salt-aging was developed. High salt concentrations (>0.15 M) were applied to screen the negative charges of the DNA backbone allowing the assembly of a densely packed ODN corona [101]. Via these methods DNA NPs are accessible with core diameters ranging from 2 to 250 nm [102,103]. Important in the context of biomedical applications and the long-term toxicity of inorganic NPs [104–106] is the fact that the Au core can also be completely removed. For that purpose the ODN was attached via a propargyl ether-modified terminal nucleotide on an Au NP template and cross-linked. Finally, the core was removed by oxidative dissolution [107].

As for the pristine DNA nanoobjects a major threat for the in-vitro and in-vivo applications of Au NPs is the digestion by nucleases. Detailed studies have been performed for these materials and the findings might be of importance for the pristine DNA assemblies as well. By incubation of DNA-Au NPs with DNAse I it was demonstrated that ds nucleic acids are more stable when bound to a core compared to pristine ds DNA [27]. The same stability was observed in an intracellular environment (C166 cells). The reason for the enhanced integrity of DNA bound to the Au NPs was investigated [108]. It turned out that not steric inhibition of binding of the nuclease was responsible for the increased stability but the high local ion concentration associated to the densely packed DNA. Pristine DNA and DNA-Au NPs exhibited comparable enzymatic digestion rates under conditions where salt concentrations do not affect the enzyme's activity. In contrast, at high salinities the degradation rate of NP-bound DNA was drastically reduced relative to unbound one. From these results it was concluded that the high local sodium ion concentration is the dominating factor for the origin of enhanced stability of DNA. In serum the stabilizing effect is further increased due to absorption of serum proteins on the surface of DNA-Au NPs and associated therewith the reduced access by nucleases.

Even more surprising than the improved integrity of DNA on the NPs was the finding that DNA-Au NPs were able to enter a large variety of cell types. Usually, transfection reagents [109,110] are required

to deliver ODNs or genes to cells due to the fact that the cell surface is negatively charged and represents a strong barrier for the negatively charged polyelectrolyte DNA due to electrostatic repulsion. Up to now it was shown that DNA-Au NPs are taken up by more than 30 cell lines, primary cells and neurons without the need for a positively charged transfection agent [94]. In view of these remarkable results with uptake of millions of NPs per cell the mechanism of this process was studied in more detail. A key requirement for pronounced uptake is a dense DNA surface layer on the particles since cellular internalization of bare citrate particles or particles passivated with BSA is orders of magnitude lower [111,112]. The influence of the core for uptake is minor since both DNA-coated iron oxide NPs as well as spherical nucleic acids (DNA NPs after core removal) exhibit high cellular uptake. The universal uptake behavior is promoted in part by membrane-bound scavenger receptors [113] which recognize specific polyanionic ligands including ODNs [114] or phosphorthioated ODNs [115] and induce receptor-mediated endocytosis. A possible uptake mechanism may look like that: First, serum proteins such as BSA adsorb to the ODN shell of the Au NPs which slightly inhibits uptake. Subsequently, the scavenger receptors bind to the DNA-Au NPs and initiate endocytosis while the serum proteins are replaced from the NP surface. A strong hint supporting this mechanism is the reduced uptake after these receptors were inhibited by their natural agonists such as poly-inosine and fucoidan [116].

Due to this favorable property profile, DNA-Au NPs were exploited for drug delivery purposes. In this context their ability for targeting was assessed first [117]. Therefore, a monoclonal antibody (mAb) recognizing human epithelium growth factor receptor 2 (HER2) was conjugated to an ODN. HER2 is part of the ErbB protein family that is involved in signaling pathways leading to increased cell proliferation and differentiation [118,119]. The mAb conjugate was hybridized with DNA-Au NPs to be connected via non-covalent bonds. The resulting DNA-Au NPs were taken up by HER2-positive cells (SKOV-3) to a much greater extent and at a faster initial rate relative to HER2-negative cells documenting the targeting effect and cell type selectivity of the conjugated mAb.

Besides equipping the DNA-Au NPs with Ab they were loaded with anticancer drugs [120]. As a starting point served DNA-Au NPs that were functionalized with an ODN carrying a terminal amine at the rim of the NP. This terminal group was functionalized with a Pt(IV) complex. Cisplatin is a well-established anticancer drug [121,122] and Pt (IV) complexes act as an attractive alternative to Pt (II) species. Pt(IV) compounds are more inert and cause less side effects relative to Pt(II)-based anticancer drugs that exhibit higher reactivity and thus lower biological stability. The Pt(IV)-loaded DNA-Au NPs were successfully internalized by cells and reduced to liberate cisplatin. This active species entered the cell nucleus and formed 1,2-d(GpG) intrastrand cross-links with genomic DNA. The effectiveness of the Pt DNA-Au NPs was superior to cisplatin in killing several kinds of cancerous cell lines. Another anticancer drug, paclitaxel, was incorporated into DNA-Au NPs [123]. This potent chemotherapeutic agent is characterized by a low solubility in aqueous media which can limit its effectiveness. Moreover, treatment regimens with this drug were limited by eventual acquirement of resistance of the cancer cells. Similar as described in the context of the Pt-loaded NPs, paclitaxel was covalently connected to the surface of DNA-Au NPs. Through the conjugation to NPs the hydrophylicity and stability of the drug was significantly increased compared to free paclitaxel. The NP-based drug delivery system was more effective in inducing apoptosis in-vitro across several cell lines and concentrations than the free active. Notably, cell death was even induced in paclitaxel-resistant MES-SA/Dx5 cells underlining the potency of DNA-Au NP systems for drug delivery.

Besides loading anticancer drugs by covalent connections to the DNA-Au NPs the chemotherapeutic agents were introduced by non-covalent bonds into the NP system [124]. Dox and actinomycin D (actD) were intercalated in pre-designed binding sites of two respective types of ds DNA-Au NPs (core diameter 15 nm) [125,126]. Regarding the liberation of the drugs from the carrier it was found for Dox that the rate constant for release was four orders of magnitude smaller than for Dox-loaded duplex DNA in solution. In stark contrast, for actD a similar rate constant for release was found for NP-loaded drug and drug bound to ds DNA. Cytotoxicity measurements employing neuroblastoma cells revealed no obvious toxicity of the unloaded DNA carriers. When loaded with the chemotherapeutic agents both vehicles showed higher toxicity at low drug concentrations but were less cytotoxic at higher concentrations compared to the freely administered actives.

In extension to intercalating Dox molecules into the nucleic acid shell of Au NPs, the carriers were equipped with a targeting function [127]. For that purpose served an aptamer that targets prostate cancer cells by recognizing prostate-specific membrane antigen (PSMA) (Fig. 15) [128]. The targeted nucleic acid NPs were internalized in LNCaP cells that express PSMA three times more than PC3 cells that are PSMA-negative. In addition to histological detection of NP uptake and quantification by inductively coupled plasma atomic emission spectroscopy, computed tomography was carried out in-vitro to prove the targeting of the NP system. At the same time these experiments document the utility of this delivery vehicle to fulfill also a bioimaging function.

Besides employing the gold core for imaging purposes, it was exploited for the stimulus-induced release of anticancer drugs [129]. The shape of the core was chosen to be rod-like (50 nm × 10 nm). The DNA shell on top was loaded with Dox and the surface was decorated with folic acid targeting units by hybridization. The modular assembly of this multifunctional carrier is illustrated in Fig. 16. Compared to spherical Au NPs their rod-like counterparts exhibit a plasmon band at higher wavelength in the near infrared (NIR) region (650–900 nm). Since NIR light can deeply penetrate tissue [130] and can be effectively converted into heat after absorption by the Au nanorods (NRs), the light-induced liberation of Dox from the DNA coated rods was successfully realized in-vitro and in-vivo. Due to the drug release, tumor growth in BALB/c nude mice was efficiently inhibited. This work represents an example of a combination of three kinds of therapy, i.e. NIR-based thermotherapy, triggered chemotherapy and targeted delivery. Although the NRs were intratumorally injected this work is the basis for further developments achieving optimal biodistribution for systematic administration. Such an optimization process is greatly facilitated by the modular assembly platform which might be easily transferred to treatments of other human diseases.

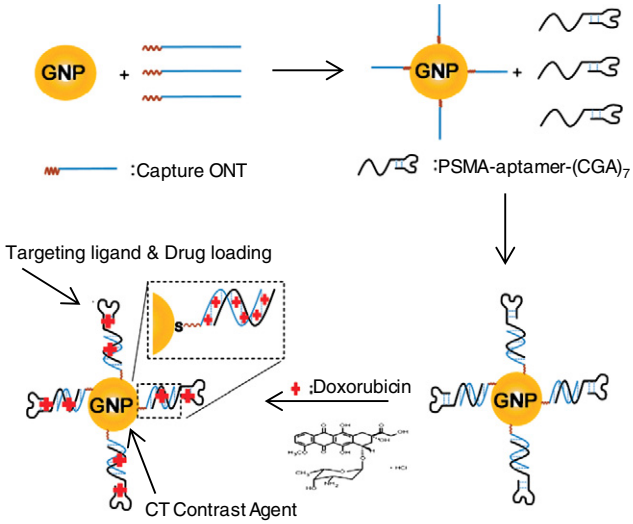

Fig. 15. Schematic representation of the assembly of targeting Dox-loaded Au NPs using the PSMA aptamer.
Reproduced with permission from [127].

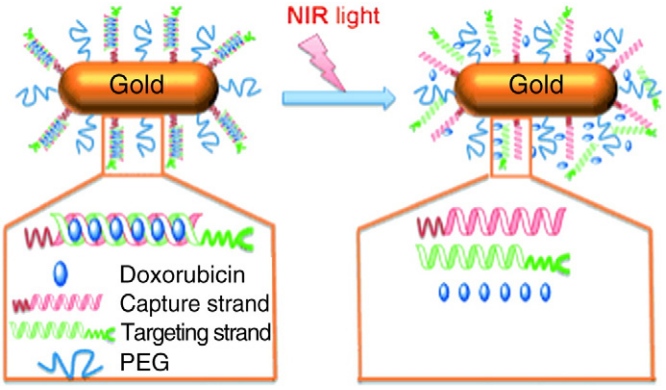

Fig. 16. Schematic representation of Au NRs for targeted Dox delivery functionalized using folic acid targeting strands. Upon irradiation with NIR light the NR is heated and induces dehybridization of the targeting and capture strand, resulting in release of the loaded drug.
Reproduced with permission from [129].

Like described for the pristine DNA nanoobjects, DNA-Au NPs were employed for immunostimulation as well [131]. For that purpose the inorganic core was functionalized with CpG motifs. Strikingly, the CpG Au NPs were more than one order of magnitude more effective in inducing TNF-α secretion compared to naked ss CpG ODNs. These experiments suggested that CpG Au NPs can act as proinflammatory stimuli in-vitro and might be a promising therapeutic tool in animals.

3.1.2. NPs composed of silica and DNA

Aside from DNA-Au nanomaterials, mesoporous silica nanoparticle (MSN) conjugates offer great opportunities for drug delivery. These structures are highly porous and thus have a high drug loading capacity. Furthermore, their pore size can be easily tailored, they are biocompatible and exhibit high thermal stability. The synthesis of MSNs proceeds through growth of triethyl orthosilicate under basic conditions onto micellar rod scaffolds that act as a template and typically are made of *n*-cetyltrimethylammonium bromide (CTAB) [132]. Afterwards the surfactant is removed under acidic conditions to yield MSNs with a diameter of around 100–200 nm and pores with sizes of 2–10 nm. Functionalized MSNs can be prepared through co-condensation with functional oligosilicates such as chlorinated or amino-modified trimethoxysilanes [133,134]. Herein the position of the functional group is controlled by the time point at which the modifiers are added. When supplementing them early in the growth process functionalities will be incorporated in the core, whereas addition at the end of the synthesis yields surface-modified MSNs.

Due to their channel architecture various types of release mechanisms for MSNs were developed. Most of these mechanisms rely on external stimuli to trigger the liberation of drugs like the presence of small molecules [135] or enzymes [136], changes in the redox potential [137] or pH [138] and photoirradiation [139]. A key role in the release process play different kinds of capping agents that include organic molecules, gold nanoparticles, polymers, antibodies and DNA. When using ODNs as gate of the channels, the most straightforward method to block the pores is by functionalization of MSNs with two complementary strands of ss DNA at the pore mouths. Hybridization results in ds DNA that effectively closes the pores and yields a nanocontainer that is responsive to both temperature changes and presence of nuclease (Fig. 17A). This simple approach was successfully used for the delivery of the hydrophobic anticancer drug camptothecin to human liver cancer cells (HepG2) and showed improved drug uptake over the free drug while the MSN itself showed no cytotoxicity [140].

When using modified ODNs as capping moieties other stimuli could be employed to release payloads. One such example is the

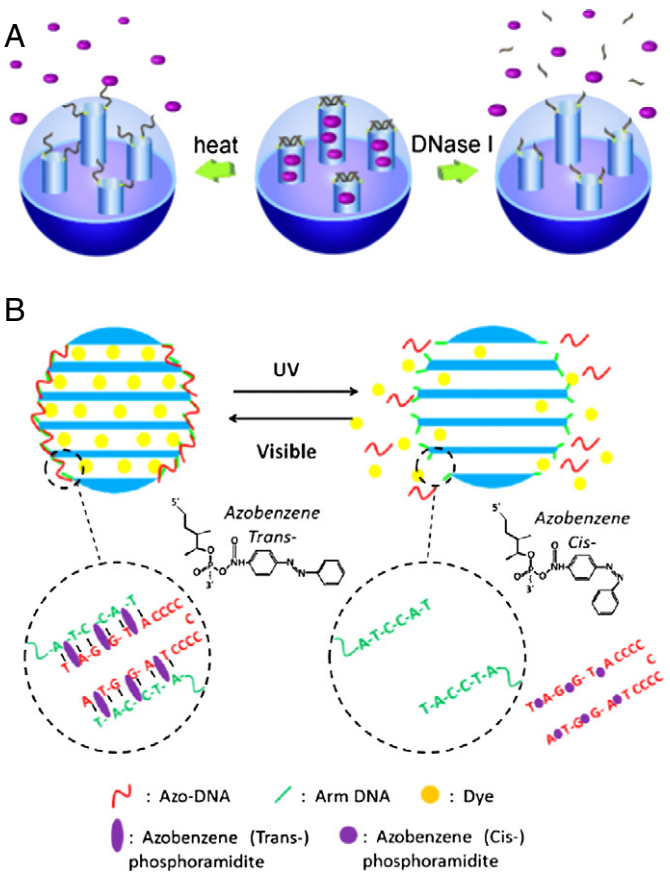

Fig. 17. (A) MSN loaded with dye and capped using ds DNA. These architectures can be employed for delivery employing temperature (left) or enzyme induced (right) release. (B) A similar approach for capping MSN that uses modified ODNs. Upon irradiation with UV light the azobenzene modification undergoes a conformational change thereby interfering with hybridization.
Reproduced with permission from [140,141].

photo-induced release of Dox that was achieved through incorporation of photoswitchable azobenzenes in the capping DNA (Fig. 17B) [141]. In the absence of light these moieties are in a *trans*-configuration and therefore allow for hybridization of two DNA strands. However, under irradiation with UV light the azobenzene undergoes isomerization into the *cis*-configuration, which interferes with hybridization. As a result, the two DNA strands separate and Dox was released. This process is reversible. Upon irradiation with visible light the pores of the MSN were closed again after sufficient drug had been released. In-vitro studies using this method were performed on CEM and A549 cells and revealed that these MSNs do not exhibit obvious cytotoxicity before irradiation with UV light. However, after irradiation cell viability dropped to only 10% showing an efficient drug release.

In an approach that used a more complex nucleic acid architecture, the DNA i-motif was employed to facilitate pH responsive release of a model compound (Fig. 18A) [142]. This special secondary structure of DNA is comprised of a single strand that folds into a quadruplex through multiple cytidines that are protonated at acidic pH [143,144]. In the quadruplex state the pores of the MSN were blocked. However, at basic pH the cytidines were deprotonated and the secondary structure was lost within minutes to facilitate release of the payload. By fabrication of NHS-activated MSNs the ss DNA coding for the i-motif was coupled to the nanoparticles. After loading of the DNA-functionalized MSNs with the model compound rhodamine B, the pH was lowered in order to close the pores. Using this simple preparation procedure loaded MSNs were obtained that showed complete release of the dye at basic pH within 24 h while less than 5% leakage was observed in the same period at acidic pH. Furthermore,

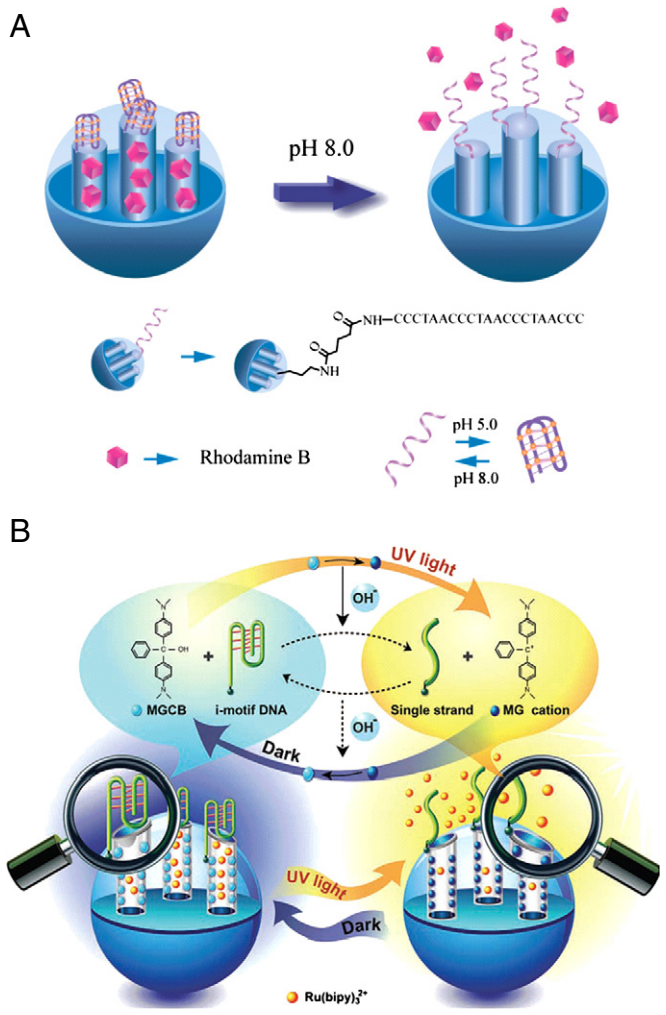

Fig. 18. (A) Loaded MSN capped with i-motif DNA. Increase of the pH results in disaggregation of the quadruplex and opening of the pores. (B) Malachite green carbinol-modified MSN for light-induced pH increase and dye release.
Reproduced with permission from [142,145].

partial release was shown by changing the pH after the desired amount of payload was liberated.

Besides utilizing changes in pH as stimulus for release, light-triggered liberation of the loaded compound was achieved using the i-motif again (Fig. 18B) [145]. For this purpose malachite green carbinol (MGCB) was immobilized on the surface of the NP after introducing the i-motif. MGCB functions as a light inducible hydroxide emitter as it dissociates into malachite green cations and OH^- upon irradiation with UV light (365 nm). The photochemical transformation creates a local increase in pH and hence induces the unfolding of the i-motif and subsequent release of the cargo. When the light is turned off, the process is reversed and the stable quadruplex is formed again to close the pores of the MSNs. Using this approach a controlled pH increase from 4.9 to 10.1 was achieved when irradiating the nanocarriers. Upon removal of the light source the initial pH value was regained after 20 min. The release of the loaded model compound ($Ru(bipy)_3^{2+}$) proved to be strongly dependent on the light conditions. Under light irradiation as much as 85% of the payload was released while in the dark only 5% leakage was observed. In addition, this approach allowed partial drug release by removing the light source after the desired amount of cargo was released.

Other DNA structures functioning as gate keepers were realized as well. To this end metal ion binding stem loop sequences were formed through hybridization to DNA functionalized MSNs allowing for Zn^{2+} and Mg^{2+} mediated release of model compounds methylene blue (MB^{2+}) and thionine (Th^+) [146]. Addition of the metal ions resulted in the formation of a catalytically active complex, called DNAzyme, that cleaves one of the strands and thereby opens the pores. Using different DNAzymes metal specific release was achieved and in a mixture of NPs controlled liberation of payloads was demonstrated. Additionally, incorporation of an aptamer in the loop sequence resulted in capped MSNs requiring two promoters to trigger release. Most importantly, release of the more relevant DOX was shown employing a Mg^{2+} and ATP dependent DNAzyme. As cancerous cells have a high metabolic activity, large amounts of ATP are present rendering this approach promising for future tumor treatment.

Apart from using the structural properties of DNA to cap the pores of MSNs, ODNs were used as anchor to attach different capping groups by employing the unique self-recognition properties of DNA. It was shown that avidin was able to function as capping agent when MSNs were functionalized with biotin modified ds DNA at the pore mouths [147]. Upon heating above the melting temperature the double strands dehybridize and avidin is removed, resulting in release of the loaded compound from the MSN. Furthermore, it was shown that the release temperature can easily be altered by changing the length of the connecting DNA. Aside from heating the whole sample, release by localized heating was also demonstrated. To this end, superparamagnetic iron oxide nanocrystals were employed that can be heated by a rapidly alternating magnetic field [148]. Hybridization of DNA functionalized MSNs with iron oxide NPs that are equipped with the complementary sequence results in loaded nanoparticles capped by DNA anchored iron oxide NPs. Additionally, the iron oxide nanoparticles do not only serve as capping agents, but also can be employed as contrast enhancing agents in magnetic resonance imaging. Important to note is that this method provides an elegant manner for liberation without the need of an invasive stimulus.

3.2. Amphiphilic DNA block copolymers

In addition to DNA NPs with an inorganic core, nanosized objects with a DNA corona and a soft interior part can be generated by employing polymeric materials. In general, amphiphilic block copolymers have been utilized frequently for drug delivery purposes [149]. Thereby, a hydrophobic polymer segment is covalently connected to a hydrophilic one. Upon microphase separation, mostly spherical aggregates are formed that exhibit a hydrophobic interior and a hydrophilic shell [150]. The core is usually exploited to load hydrophobic drugs or for encapsulation of toxic actives to prevent them from harming healthy tissue. The shell is often composed of polyethylene glycol because of its resistance towards protein adsorption and the prevention of immunogenicity [151]. Alternatively, stimulus responsive water soluble polymer segments are found in the corona of the micelles allowing the particles to react towards changes in their environment to improve the performance of the carrier system.

Another way to introduce function into these micellar systems is the utilization of DNA as a constituent part of the amphiphilic block copolymer. Several ways have been established to synthesize DNA block copolymers. Early methods to access linear DNA block copolymers (DBCs) relied on coupling the ODN segment to the hydrophobic polymer in solution which did not result in good coupling yields [32]. A more efficient approach relied on attaching the nucleic acid segment to the DNA unit on the solid phase. Therefore, the ODN was synthesized by conventional phosphoramidite chemistry on controlled porous glass or a polymeric support [152]. Afterwards, a phosphoramidite polymer, which was obtained by phosphitylation of its terminal hydroxyl group, was coupled to the detritylated end of the ODN that was still attached to the solid phase. After removal of the protective groups and cleavage from the support amphiphilic DBCs were obtained in good yields [38]. Other ways for the

fabrication of DBCs rely on molecular biology methods employing different enzymes [36,153–155].

After detailing their preparation methods, the self-assembly of amphiphilic DBCs will be discussed. When these materials are introduced into buffer they form spherical micelles. The size of these nanoobjects can be easily controlled by adjusting the lengths of the different polymer blocks. Just to give an example, a DBC consisting of a ODN 22mer connected to a poly(propylene oxide) (PPO) segment of weight average molecular weight (M_w) of 6800 g/mol results in micelles with a hydrodynamic radius of 10 nm. When the DNA block is extended to 84 nucleotides a diameter of 23 nm is obtained [155]. The geometry of the spherical aggregates could be switched into rod-like objects by a simple hybridization procedure [156]. Therefore, the ss DNA-*b*-PPO micelles were mixed with long DNA templates that encode several times the complementary sequence of the micelle corona inducing a transformation into rod-like micelles. Watson–Crick base pairing aligned the hydrophobic polymer segments along the DNA double helix, which resulted in selective dimer formation (Fig. 19). Even the length of the resulting nanostructures could be precisely adjusted by the number of nucleotides of the templates. Rod-like particles with lengths between 30 and 37 nm were generated. This study demonstrated that structurally well-defined DNA nanoobjects can not only be produced by Watson–Crick base paring as described in the context of pristine DNA assemblies but also by interactions of hydrophobic polymers. The use of hydrophobic interactions represents a new principle for DNA nanoconstruction.

The spherical and rod-like DBC nanostructures were investigated in regard to their interaction with cells. Uptake studies into the cancerous Caco 2 cell line revealed an internalization behavior that is strongly dependent on the geometry of the nanostructures [157]. It turned out that the rod-like aggregates were taken up to a much greater extent than ss and ds spherical micelles. In the context of drug delivery this is an important finding because it suggests that shape is an important design criterion for drug carriers. It is noteworthy that all the DNA aggregates were taken up much better than the ss and ds DNA controls. The same finding that nanoparticles with a high nucleic acid density are efficiently incorporated into cells was previously observed for DNA-Au NPs and was later seen for pristine DNA nanoobjects as well (vide supra).

After investigating the non-directed uptake of DBC aggregates, these systems were employed for targeted chemotherapeutic drug delivery [158]. For that purpose ODN-modified targeting units (folic acid) were "clicked" into the spherical micelle corona by hybridization, allowing perfect control of surface functionalities of the nanoparticle system. When folate is conjugated to the 5′-end of the ODN it is present at the surface of the micelles (Fig. 20A). If the targeting moiety is connected to the 3′-end it is located at the inside of the DBC aggregates. In addition, different stoichiometries of ODN-folate conjugates to micelles allowed control of number of targeting unit per micelle. The aggregation number of this DNA–*b*-PPO system was determined to be 25 resulting in an average of 25 folate units on the surface of the DBC vehicles when fully hybridized with 5′-functionlized ODNs. Cell culture experiments with Caco 2 cells revealed that cellular uptake strongly depends on the density of targeting units on the surface of the carriers. Receptor-mediated uptake is most efficient for the design with the maximum number of folate groups on the surface. As convenient the DBC aggregates are equipped with surface functionalities, as simple the drug loading can be carried out. By just mixing the hydrophobic anticancer drug Dox with the micelles, the cargo accumulates in the core of the DBC aggregates (Fig. 20B). When the DBC particles that were most efficient in targeting were administered with the cytotoxic payload to cancer cells in-vitro the Caco 2 cells were efficiently killed, whereas the NPs themselves did not show any toxicity.

These experiments qualify the amphiphilic DBCs as delivery system with high future potential. The hydrophobic polymer organizes the ss ODN moieties to form a dense ss DNA corona that can be easily equipped with many different functionalities by hybridization as proven for targeting and bioimaging agents. Moreover, the core of the DNA nanoparticles can be exploited for the loading with hydrophobic cargo. In this way a combinatorial testing of different compositions of DBC-based drug delivery systems becomes feasible. Similarly to the DBC micelle system, aptamers recognizing Ramos cells were assembled into micelles through implementation of a hydrophobic moiety at one end of the ODN. Interestingly, due to the multimerization of the aptamer sequence an increased binding of the micelles compared to the pristine nucleic acid sequence was achieved [159].

In future experiments, especially during in-vivo applications, the DBC aggregates, like any other micelle system, might disaggregate due to dilution upon administration. For that reason we stabilized DBC aggregates by adding a hydrophobic cross-linker to the core that was photo-polymerized [160]. At the same time the DNA–*b*-PPO system was blended with Pluronics, a triblock copolymer with a PEG–*b*-PPO–*b*-PEG architecture. As a result, the corona of the micelle corona consists of ODN and PEG units. It was proven that the PEG moieties at the surface of the aggregates did not interfere with hybridization. In this way, a stable DNA nanoparticle system was generated combining a PEG-stealth function with all the favorable properties of pristine DBC micelles.

A second way of stabilizing DBC aggregates is encapsulation of the whole nanoobject. This goal was successfully realized with virus capsids. Micelles of amphiphilic DBCs acted as efficient template for the formation of virus-like particles of the Cowpea Chlorotic Mottle

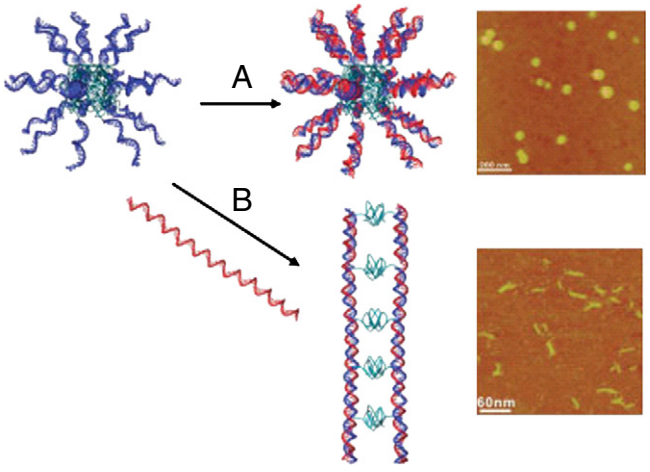

Fig. 19. Preparation of soft DNA nanoparticles with different shapes and the corresponding AFM pictures of the nanoobjects. (A) Base pairing of ss DNA-*b*-PPO micelles with a short complementary sequence yields micelles with a ds corona maintaining the overall spherical shape of the aggregates. (B) Hybridization with long DNA templates results in rod-like micelles consisting of two parallel aligned double helices.

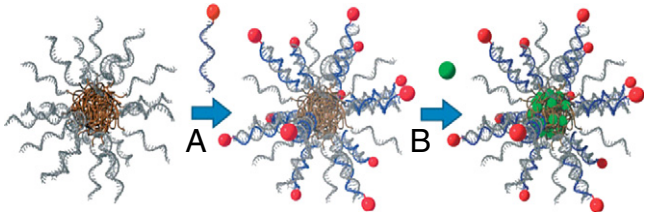

Fig. 20. Schematic representation of the drug delivery system based on DNA block copolymers. (A) Targeting units (red dots) that are connected to the complementary sequence of the micelles are hybridized to equip the nanoparticle surface with folate moieties. (B) The anticancer drug (green dots) is loaded into the core of the micelles. Due to hydrophobic interactions of Doxorubicin with PPO the drug accumulates in the interior of the block copolymer aggregates.

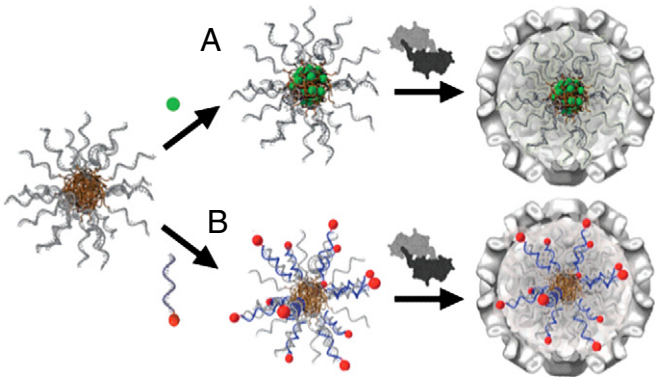

Fig. 21. DNA micelle-templated virus capsid formation. (A) Loading of hydrophobic molecules (green) into the core. (B) Hydrophilic moieties (red) are attached to the DNA NP by hybridization. Subsequently, coat proteins encapsulate the micelle by a simple mixing process at neutral pH.

Virus (CCMV) [161]. Under neutral pH CCMV coat protein dimers self-assemble into T = 1 and T = 2 particles consisting of 90 and 120 proteins, respectively. The resulting nanoobjects exhibit a diameter of approximately 20 nm. The incorporation of hydrophilic and hydrophobic payloads was achieved in a very simple manner similar as described earlier for the DBC drug delivery system (Fig. 21). Hydrophobic compounds, like pyrene, were accumulated in the core of the micelles during preparation of DBC micelles. Subsequently, the loaded micelles were incorporated into CCMV particles. For the loading of hydrophilic compounds the cargo was conjugated to complementary ODNs to that of DBC particles prior to the encapsidation process. The encapsulation was verified by several techniques including TEM, FPLC, UV/Vis and fluorescence spectroscopy.

While amphiphilic DBCs are superb materials for the preparation of functionalized micelles they were also employed in the context of vesicle systems. DNA–*b*-PPO was stably incorporated into the phospholipid membrane of vesicles (Fig. 22) [162]. In this way, the containers are encoded with sequence information. The ODNs present on the surface were used for anchoring a photosensitizer by hybridization. Upon light irradiation the PPO was oxidized leading to leakage in the membrane and cargo release. It was even demonstrated that in mixtures of vesicles payload is only released when sequence specific hybridization takes place. Liposomes lacking the code for photo-sensitizer hybridization remain unaffected.

When vesicles were functionalized with an aptamer recognizing cancerous cells, targeted liposomes could be successfully delivered [163]. In the same work the binding of the aptamer to the cell surface could be instantaneously inhibited and disrupted by addition of the complement of the aptamer sequence.

While in DBC micelles and DBC encoded vesicles the polymer was employed to organize a ss DNA moiety by hydrophobic interactions the opposite allocation of functions was realized. A DNA cube with ss regions was employed as a scaffold to place DBCs in a predefined manner in space (Fig. 23) [164]. In this way, upon hybridization of DBCs, synthetic polymer units could be placed at various corners of the cube indicating that with the help of DNA nanotechnology synthetic macromolecules can be programmably positioned in 3D on a DNA scaffold. Moreover, the decoration of the cube with polymer units increased the nuclease resistance compared to non-polymer containing DNA cages. These hybrid structures like many of the above mentioned DBC systems represent promising precision materials for biomedical and drug delivery applications.

4. Conclusion

DNA nanotechnology has developed into an independent field of research in the recent years. Dramatic improvements have been booked regarding the accessibility of possible structures. One can firmly state that nowadays almost any 2D or 3D shaped nanoobject is achievable with DNA as a building block. In contrast to many other self-assembling systems the geometry and size of DNA nanoarchitectures can be designed very accurately due to the well-known self-recognition properties of DNA and the knowledge of the exact structure of the double helix on the atomic level. Without any doubt, the DNA origami technique is nowadays the one giving the highest degree of flexibility regarding the structural variety. Although DNA nanostructures being composed of nucleic acid hybrid materials allow less structural control and variability they give the opportunity for the implementation of extra functionality.

Both types of materials, pristine DNA nanoobjects and DNA hybrid structures, were exploited in the context of biomedical applications. DNA nanoobjects were employed as scaffolds to act as a drug carrier or to display functionalities that induce immunostimulation. Why are nucleic acid nanostructures so appealing for those potential applications? There are several answers to this question. One obvious one

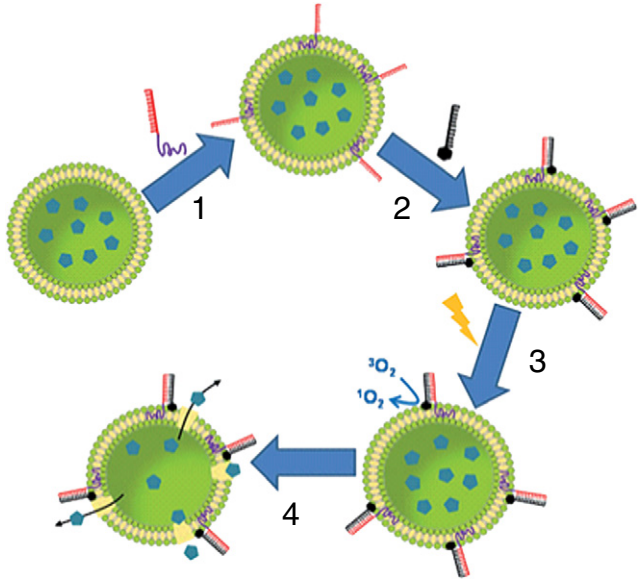

Fig. 22. Illustration of selective cargo release from DBC-decorated phospholipid vesicles. (1) DBCs are stably anchored in unilamellar lipid vesicles; (2) DBC-decorated vesicles are functionalized with conjugated ODN-photosensitizers by hybridization; (3) singlet oxygen is generated by light irradiation; and (4) selective cargo release is induced by the oxidative effect of singlet oxygen.

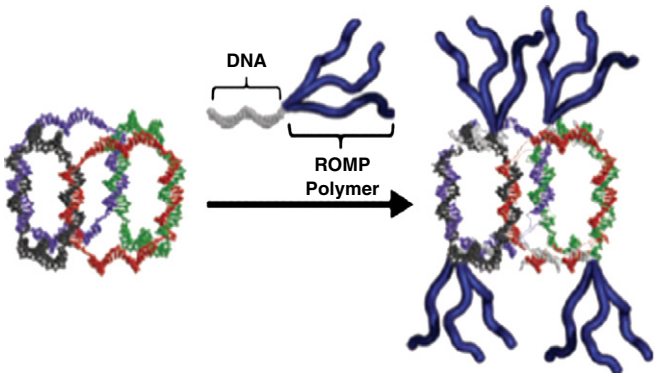

Fig. 23. Schematic design of a polymer-conjugated DNA cube. The cube is designed to hybridize with four DNA polymer conjugates, two on both the top and bottom face. In each face the polymers are directed perpendicular to each other through site-specific hybridization in order to minimize steric hindrance.
Reproduced with permission from [163].

is that the DNA nanostructures can be decorated with a multitude of functionalities including drugs, targeting moieties and stealth units. With the help of the DNA scaffold these entities can be positioned with a similar accuracy as the DNA itself. The great need for multifunctional carriers in the context of drug delivery vehicles does not need to be further explained here. Another striking feature of the DNA nanoobjects is their modular fabrication relying on self-assembly. Only a few or a large number of building blocks are mixed together in a single step resulting in the formation of the desired nanostructure. In this way, variations of the design or the decoration of the carrier can be easily achieved. In stark contrast, other carrier scaffolds like dendrimers mostly require cumbersome multistep synthesis which does not allow testing of many designs and structural variations. It needs to be mentioned here that the DNA sequences need to be synthesized as well, but their fabrication relies on well-established automated synthesis methods and ODNs are available from commercial suppliers. Moreover, via the self-assembly process with DNA a large size range is covered ranging from only a few nanometer like the DNA tetrahedron to structures in the micrometer scale like the extended DNA tubes. Another striking feature suggesting the use of DNA-based carrier systems is that they are taken up by cells without the need for a transfection agent. This was first discovered for DNA-Au NPs and seems to be true for many other DNA nanostructures as well that are composed of high density DNA like DBC micelles, DNA polyhedra and DNA origami tubes. An equally important characteristic for their biomedical application is their low immunogenicity. Several examples in this review demonstrate that once the DNA is tightly compressed in a dense DNA scaffold immunogenicity is low like shown for some pristine DNA and DNA-Au NPs. Moreover, for all DNA-based materials presented in this review no or only a low toxicity was found in the absence of the payload or stimulants, while they greatly improve the performance of the active compounds.

While DNA nanostructures from pristine nucleic acids and from DNA hybrid material have several common features they also exhibit differences. Pristine DNA nanostructures mostly allow more structural control if one thinks e.g. of the DNA origami method compared to DNA-Au NPs or DBC micelles. On the other hand DNA-Au NPs and DBC aggregates allow much higher densities of surface units compared to pristine nucleic acid structures. For the former ones ss DNA is arranged in space by an Au- or a hydrophobic polymer core while for the latter ones overhangs of ss DNA can be introduced into double helical structures with lower frequency.

Another good reason for testing DNA nanostructures for the purpose of drug delivery is the large flexibility of how drugs can be loaded into the DNA carrier. As demonstrated for chemotherapeutics like Dox intercalation into the double helix is a valuable method. But drugs can also be chemically attached to the surface of the nanocarriers which at the same time helps increasing the solubility of a drug. Alternatively, hydrophobic actives might be incorporated into the lipophilic core of DBC aggregates. Another loading strategy consists of hybridizing drug-ODN conjugates onto single stranded sites of the DNA carrier.

While DNA nanoobjects offer several possibilities for drug incorporation they allow superb control over release as well. Due to the specific hydrogen bonds formed between adenine and thymine and guanosine and cytosine the melting temperature between two complementary DNA strands can be precisely controlled. This feature can be exploited for the temperature-controlled release of compounds that are attached to the strands or that are intercalated. Likewise, the hydrogen bonding in DNA can be exploited for sequence specific release with the help of DNA or RNA input strands. In this case one of the strands needs to contain a toehold overhang that allows strand exchange and therewith release. Other DNA-mediated release mechanisms rely on specific DNA sequences. The i-motif is switching in response to pH between a compact quadruplex structure and an extended single stranded conformation. This allowed controlled release when those structures are introduced as valves at the tip of silica channels. Light as a stimulus for drug release is another option. In case of silica particles a photobase induces local pH changes and switching of the i-motif. On the surface of liposomes photosensitizer units can be hybridized and exploited for sequence-specific release of cargo.

The summary above shows that pristine DNA nanostructures and nanoobjects composed of DNA hybrid materials offer unprecedented control over structure and functionality in a biological or cellular environment. Several in-vitro studies have shown the exciting properties of nano-sized nucleic acid-based carrier materials. However, the scope of these investigations is still limited. The focus has been on two main areas, i.e. usage of DNA-based carriers for cancer treatment and as immunostimulants exploiting the multimerization of the CpG motif (Table 1). Further in-vitro experiments might extend the applications of this carrier family to other indications and diseases. Even more important for the demonstration of the great potency of DNA nanomaterials in the biomedicine arena is the establishment of these vehicles in-vivo. Such experiments are still scarce but one can imagine that more successful examples will be presented soon due to the fact that the field of DNA-based carriers has gained great momentum in the very recent years. In the near future it is expected that the scope and limitations of such delivery vehicles regarding indications, targeting-ability, toxicity, immunogenicity, pharmacokinetics and pharmacological efficacy (local pharmacological effects, toxicity in non-target tissue, and overall effect on disease progression) will be shown. This preclinical validation calls for fabrication of DNA nanomaterials of pharmaceutical grade and at larger scales. For pristine nucleic acids and DNA block copolymers these requirements can be met with established techniques such as solid-phase synthesis and automated HPLC. One example thereof is the commercially available anti-VEGF nucleic acid aptamer used for treatment of wet age related macular degeneration [30]. In regard to inorganic

Table 1
Overview of DNA nanostructures equipped with CpG motifs for immunostimulation.

Class	DNA nanoobject	Reference	Immunostimulatory effect
Pristine DNA	Tetrahedron	[59]	Tetrahedra functionalized with 4 CpG motifs increase TNF-α and IL-6 concentrations by a factor of 13 and 35, respectively, compared to ds CpG motifs.
		[60]	Doubled antibody response and significantly higher levels of memory B cells were found when using the NP enhanced vaccines compared to the unassembled individual components.
	Dendrimers	[64]	Y shaped structures cause a 1.5- to 3-fold increase in release of TNF-α and IL-6, respectively, compared to ds CpG.
		[65]	2nd and 3rd dendrimer generations strongly increase TNF-α levels by a factor of 7 and 22, respectively, compared to ds CpG. IL-6 concentrations were approx. increased by a factor of 3 (G2) and 5 (G3).
	Polypods	[66]	With increasing branching of the pods an enhanced stimulation was found for both TNF-α and IL-6. For the prior cytokine a 5-fold to 400-fold increase was observed compared to ds DNA. For IL-6 release induced by ds DNA the values were below the detection limit.
	DNA tubes	[52]	TLR9 specific immune responses were triggered using CpG decorated nanotubes with a fivefold increase in IL-6 concentrations compared to undecorated tubes.
DNA hybrids	DNA-Au NPs	[130]	Strongly stimulated cytokine release in comparison with non-NP CpG motifs. In relation to ss CpG, a 16- and 10-fold increase in TNF-α and IL-6 concentrations was observed, respectively.

DNA hybrids, probably more effort is necessary to achieve the homogeneity and scale established in pharmaceutical industry. These considerations help to realize the long-term goal of this branch of nanomedicine research which is to identify promising nucleic acid-based carrier systems and bring them into the clinic. However, the latter endeavor is beyond a short time frame.

References

[1] J.D. Watson, F.H.C. Crick, The structure of DNA, Cold Spring Harb. Symp. Quant. Biol. 18 (1953) 123–131.
[2] L.M. Smith, Nanostructures — the manifold faces of DNA, Nature 440 (2006) 283–284.
[3] N.C. Seeman, Nucleic-acid junctions and lattices, J. Theor. Biol. 99 (1982) 237–247.
[4] N.C. Seeman, DNA in a material world, Nature 421 (2003) 427–431.
[5] J. Chen, N.C. Seeman, Synthesis from DNA of a molecule with the connectivity of a cube, Nature 350 (1991) 631–633.
[6] E. Winfree, F.R. Liu, L.A. Wenzler, N.C. Seeman, Design and self-assembly of two-dimensional DNA crystals, Nature 394 (1998) 539–544.
[7] A. Kuzuya, R.S. Wang, R.J. Sha, N.C. Seeman, Six-helix and eight-helix DNA nanotubes assembled from half-tubes, Nano Lett. 7 (2007) 1757–1763.
[8] P.W.K. Rothemund, Folding DNA to create nanoscale shapes and patterns, Nature 440 (2006) 297–302.
[9] E.S. Andersen, M. Dong, M.M. Nielsen, K. Jahn, R. Subramani, W. Mamdouh, M.M. Golas, B. Sander, H. Stark, C.L. Oliveira, J.S. Pedersen, V. Birkedal, F. Besenbacher, K.V. Gothelf, J. Kjems, Self-assembly of a nanoscale DNA box with a controllable lid, Nature 459 (2009) 73–76.
[10] Y. Ke, S. Lindsay, Y. Chang, Y. Liu, H. Yan, Self-assembled water-soluble nucleic acid probe tiles for label-free RNA hybridization assays, Science 319 (2008) 180–183.
[11] S. Rinker, Y. Ke, Y. Liu, R. Chhabra, H. Yan, Self-assembled DNA nanostructures for distance-dependent multivalent ligand–protein binding, Nat. Nanotechnol. 3 (2008) 418–422.
[12] A.V. Pinheiro, D.R. Han, W.M. Shih, H. Yan, Challenges and opportunities for structural DNA nanotechnology, Nat. Nanotechnol. 6 (2011) 763–772.
[13] C. Zhang, M. Su, Y. He, X. Zhao, P.A. Fang, A.E. Ribbe, W. Jiang, C.D. Mao, Conformational flexibility facilitates self-assembly of complex DNA nanostructures, Proc. Natl. Acad. Sci. U. S. A. 105 (2008) 10665–10669.
[14] D.E. Ingber, Tensegrity: the architectural basis of cellular mechanotransduction, Annu. Rev. Physiol. 59 (1997) 575–599.
[15] D. Liu, M.S. Wang, Z.X. Deng, R. Walulu, C.D. Mao, Tensegrity: construction of rigid DNA triangles with flexible four-arm DNA junctions, J. Am. Chem. Soc. 126 (2004) 2324–2325.
[16] Z. Li, B. Wei, J. Nangreave, C. Lin, Y. Liu, Y. Mi, H. Yan, A replicable tetrahedral nanostructure self-assembled from a single DNA strand, 131 (2009) 13093–13098.
[17] R.P. Goodman, I.A.T. Schaap, C.F. Tardin, C.M. Erben, R.M. Berry, C.F. Schmidt, A.J. Turberfield, Rapid chiral assembly of rigid DNA building blocks for molecular nanofabrication, Science 310 (2005) 1661–1665.
[18] W.M. Shih, J.D. Quispe, G.F. Joyce, A 1.7-kilobase single-stranded DNA that folds into a nanoscale octahedron, Nature 427 (2004) 618–621.
[19] D. Bhatia, S. Mehtab, R. Krishnan, S.S. Indi, A. Basu, Y. Krishnan, Icosahedral DNA nanocapsules by modular assembly, Angew. Chem. Int. Ed. 48 (2009) 4134–4137.
[20] Y. He, T. Ye, M. Su, C. Zhang, A.E. Ribbe, W. Jiang, C.D. Mao, Hierarchical self-assembly of DNA into symmetric supramolecular polyhedra, Nature 452 (2008) 198–201.
[21] C.A. Mirkin, R.L. Letsinger, R.C. Mucic, J.J. Storhoff, A DNA-based method for rationally assembling nanoparticles into macroscopic materials, Nature 382 (1996) 607–609.
[22] D. Nykypanchuk, M.M. Maye, D. van der Lelie, O. Gang, DNA-guided crystallization of colloidal nanoparticles, Nature 451 (2008) 549–552.
[23] R.J. Macfarlane, B. Lee, M.R. Jones, N. Harris, G.C. Schatz, C.A. Mirkin, Nanoparticle superlattice engineering with DNA, Science 334 (2011) 204–208.
[24] J.I. Cutler, E. Auyeung, C.A. Mirkin, Spherical nucleic acids, J. Am. Chem. Soc. 134 (2012) 1376–1391.
[25] J.J. Storhoff, R. Elghanian, R.C. Mucic, C.A. Mirkin, R.L. Letsinger, One-pot colorimetric differentiation of polynucleotides with single base imperfections using gold nanoparticle probes, J. Am. Chem. Soc. 120 (1998) 1959–1964.
[26] D.S. Seferos, D.A. Giljohann, H.D. Hill, A.E. Prigodich, C.A. Mirkin, Nano-flares: probes for transfection and mRNA detection in living cells, 129 (2007) 15477–15479.
[27] N.L. Rosi, Oligonucleotide-modified gold nanoparticles for intracellular gene regulation, Science 312 (2006) 1027–1030.
[28] J. Dobson, Gene therapy progress and prospects: magnetic nanoparticle-based gene delivery, Gene Ther. 13 (2006) 283–287.
[29] M. Lemaitre, B. Bayard, B. Lebleu, Specific antiviral activity of a poly(L-lysine)-conjugated oligodeoxyribonucleotide sequence complementary to vesicular stomatitis-virus N-protein messenger-RNA initiation site, Proc. Natl. Acad. Sci. U. S. A. 84 (1987) 648–652.
[30] J.P. Leonetti, G. Degols, P. Milhaud, C. Gagnor, M. Lemaitre, B. Lebleu, Antiviral activity of antisense oligonucleotides linked to poly(L-lysine) — targets on genomic RNA and or messenger-RNA of vesicular stomatitis-virus, Nucleosides Nucleotides 8 (1989) 825–828.
[31] Preclinical and phase 1A clinical evaluation of an anti-VEGF pegylated aptamer (EYE001) for the treatment of exudative age-related macular degeneration, Retina 22 (2002) 143–152.
[32] J.H. Jeong, T.G. Park, Novel polymer-DNA hybrid polymeric micelles composed of hydrophobic poly(D,L-lactic-co-glycolic acid) and hydrophilic oligonucleotides, Bioconjug. Chem. 12 (2001) 917–923.
[33] Z.Y. Zhao, L.Y. Wang, Y. Liu, Z.Q. Yang, Y.M. He, Z.B. Li, Q.H. Fan, D.S. Liu, pH-induced morphology-shifting of DNA-b-poly(propylene oxide) assemblies, Chem. Commun. 48 (2012) 9753–9755.
[34] M.P. Chien, A.M. Rush, M.P. Thompson, N.C. Gianneschi, Programmable shape-shifting micelles, Angew. Chem. Int. Ed. 49 (2010) 5076–5080.
[35] M.D. Costioli, I. Fisch, F. Garret-Flaudy, F. Hilbrig, R. Freitag, DNA purification by triple-helix affinity precipitation, Biotechnol. Bioeng. 81 (2003) 535–545.
[36] M. Safak, F.E. Alemdaroglu, Y. Li, E. Ergen, A. Herrmann, Polymerase chain reaction as an efficient tool for the preparation of block copolymers, Adv. Mater. 19 (2007) 1499–1505.
[37] G. Tong, J.M. Lawlor, G.W. Tregear, J. Haralambidis, The synthesis of oligonucleotide polyamide conjugate molecules suitable as PCR primers, J. Org. Chem. 58 (1993) 2223–2231.
[38] F.E. Alemdaroglu, K. Ding, R. Berger, A. Herrmann, DNA-templated synthesis in three dimensions: introducing a micellar scaffold for organic reactions, Angew. Chem. Int. Ed. 45 (2006) 4206–4210.
[39] M. Kwak, J. Gao, D.K. Prusty, A.J. Musser, V.A. Markov, N. Tombros, M.C.A. Stuart, W.R. Browne, E.J. Boekema, G. ten Brinke, H.T. Jonkman, B.J. van Wees, M.A. Loi, A. Herrmann, DNA block copolymer doing it all: from selection to self-assembly of semiconducting carbon nanotubes, Angew. Chem. Int. Ed. 50 (2011) 3206–3210.
[40] R. Duncan, The dawning era of polymer therapeutics, Nat. Rev. Drug Discov. 2 (2003) 347–360.
[41] P. Tanner, P. Baumann, R. Enea, O. Onaca, C. Palivan, W. Meier, Polymeric vesicles: from drug carriers to nanoreactors and artificial organelles, Acc. Chem. Res. 44 (2011) 1039–1049.
[42] Y. Kakizawa, K. Kataoka, Block copolymer micelles for delivery of gene and related compounds, Adv. Drug Deliv. Rev. 54 (2002) 203–222.
[43] S. Ganta, H. Devalapally, A. Shahiwala, M. Amiji, A review of stimuli-responsive nanocarriers for drug and gene delivery, J. Control. Release 126 (2008) 187–204.
[44] M.J. Campolongo, S.J. Tan, J.F. Xu, D. Luo, DNA nanomedicine: engineering DNA as a polymer for therapeutic and diagnostic applications, Adv. Drug Deliv. Rev. 62 (2010) 606–616.
[45] J.-W. Keum, J.-H. Ahn, H. Bermudez, Design, assembly, and activity of antisense DNA nanostructures, Small 7 (2011) 3529–3535.
[46] K.A. Whitehead, R. Langer, D.G. Anderson, Knocking down barriers: advances in siRNA delivery, Nat. Rev. Drug Discov. 8 (2009) 129–138.
[47] P. Guo, O. Coban, N.M. Snead, J. Trebley, S. Hoeprich, S. Guo, Y. Shu, Engineering RNA for targeted siRNA delivery and medical application, Adv. Drug Deliv. Rev. 62 (2010) 650–666.
[48] M.J. Campolongo, S.J. Tan, J. Xu, D. Luo, DNA nanomedicine: engineering DNA as a polymer for therapeutic and diagnostic applications, Adv. Drug Deliv. Rev. 62 (2010) 606–616.
[49] E. Katz, I. Willner, Integrated nanoparticle-biomolecule hybrid systems: synthesis, properties, and applications, Angew. Chem. Int. Ed. 43 (2004) 6042–6108.
[50] R.P. Goodman, R.M. Berry, A.J. Turberfield, The single-step synthesis of a DNA tetrahedron, Chem. Commun. (2004) 1372–1373.
[51] C. Zhang, C. Tian, X. Li, H. Qian, C. Hao, W. Jiang, C. Mao, Reversibly switching the surface porosity of a DNA tetrahedron, J. Am. Chem. Soc. 134 (2012) 11998–12001.
[52] A.S. Walsh, H. Yin, C.M. Erben, M.J.A. Wood, A.J. Turberfield, DNA cage delivery to mammalian cells, ACS Nano 5 (2011) 5427–5432.
[53] V.J. Schuller, S. Heidegger, N. Sandholzer, P.C. Nickels, N.A. Suhartha, S. Endres, C. Bourquin, T. Liedl, Cellular immunostimulation by CpG-sequence-coated DNA origami structures, ACS Nano 5 (2011) 9696–9702.
[54] G.J. Weiner, H.M. Liu, J.E. Wooldridge, C.E. Dahle, A.M. Krieg, Immunostimulatory oligodeoxynucleotides containing the CpG motif are effective as immune adjuvants in tumor antigen immunization, Proc. Natl. Acad. Sci. U. S. A. 94 (1997) 10833–10837.
[55] S. Bauer, H. Wagner, Bacterial CpG-DNA licenses TLR9, Curr. Top. Microbiol. Immunol. 270 (2002) 145–154.
[56] S. Rothenfusser, E. Tuma, S. Endres, G. Hartmann, Plasmacytoid dendritic cells: the key to CpG, Hum. Immunol. 63 (2002) 1111–1119.
[57] D.E. Fonseca, J.N. Kline, Use of CpG oligonucleotides in treatment of asthma and allergic disease, Adv. Drug Deliv. Rev. 61 (2009) 256–262.
[58] J. Vollmer, A.M. Krieg, Immunotherapeutic applications of CpG oligodeoxynucleotide TLR9 agonists, Adv. Drug Deliv. Rev. 61 (2009) 195–204.
[59] D.M. Klinman, Immunotherapeutic uses of CpG oligodeoxynucleotides, Nat. Rev. Immunol. 4 (2004) 248–257.
[60] J. Li, H. Pei, B. Zhu, L. Liang, M. Wei, Y. He, N. Chen, D. Li, Q. Huang, C. Fan, Self-assembled multivalent DNA nanostructures for noninvasive intracellular delivery of immunostimulatory CpG oligonucleotides, ACS Nano 5 (2011) 8783–8789.
[61] X. Liu, Y. Xu, T. Yu, C. Clifford, Y. Liu, H. Yan, Y. Chang, A DNA nanostructure platform for directed assembly of synthetic vaccines, Nano Lett. 12 (2012) 4254–4259.
[62] H. Pei, L. Liang, G. Yao, J. Li, Q. Huang, C. Fan, Reconfigurable three-dimensional DNA nanostructures for the construction of intracellular logic sensors, Angew. Chem. Int. Ed. 51 (2012) 9020–9024.
[63] Y.G. Li, Y.D. Tseng, S.Y. Kwon, L. D'Espaux, J.S. Bunch, P.L. Mceuen, D. Luo, Controlled assembly of dendrimer-like DNA, Nat. Mater. 3 (2004) 38–42.
[64] M. Nishikawa, M. Matono, S. Rattanakiat, N. Matsuoka, Y. Takakura, Enhanced immunostimulatory activity of oligodeoxynucleotides by Y-shape formation, Immunology 124 (2008) 247–255.

[65] S. Rattanakiat, M. Nishikawa, H. Funabashi, D. Luo, Y. Takakura, The assembly of a short linear natural cytosine-phosphate-guanine DNA into dendritic structures and its effect on immunostimulatory activity, Biomaterials 30 (2009) 5701–5706.
[66] K. Mohri, M. Nishikawa, N. Takahashi, T. Shiomi, N. Matsuoka, K. Ogawa, M. Endo, K. Hidaka, H. Sugiyama, Y. Takahashi, Y. Takakura, Design and development of nanosized DNA assemblies in polypod-like structures as efficient vehicles for immunostimulatory CpG motifs to immune cells, ACS Nano 6 (2012) 5931–5940.
[67] M. Chang, C.S. Yang, D.M. Huang, Aptamer-conjugated DNA icosahedral nanoparticles as a carrier of doxorubicin for cancer therapy, ACS Nano 5 (2011) 6156–6163.
[68] M. Brayman, A. Thathiah, D.D. Carson, MUC1: a multifunctional cell surface component of reproductive tissue epithelia, Reprod. Biol. Endocrinol. 2 (2004) 4.
[69] S.J. Gendler, MUC1, the renaissance molecule, J. Mammary Gland Biol. Neoplasia 6 (2001) 339–353.
[70] N.L. Bartlett, G.R. Petroni, B.A. Parker, N.D. Wagner, J.P. Gockerman, G.A. Omura, G.P. Canellos, M. Robert, J.L. Johnson, B.A. Peterson, Dose-escalated cyclophosphamide, doxorubicin, vincristine, prednisone, and etoposide (CHOPE) chemotherapy for patients with diffuse lymphoma: Cancer and Leukemia Group B studies 8852 and 8854, Cancer 92 (2001) 207–217.
[71] J.H. Edmonson, I.A. Petersen, T.C. Shives, M.R. Mahoney, M.G. Rock, M.G. Haddock, F.H. Sim, W.J. Maples, M.I. O'Connor, L.L. Gunderson, M.L. Foo, D.J. Pritchard, J.C. Buckner, S.L. Stafford, Chemotherapy, irradiation, and surgery for function-preserving therapy of primary extremity soft tissue sarcomas: initial treatment with ifosfamide, mitomycin, doxorubicin, and cisplatin plus granulocyte macrophage-colony-stimulating factor, Cancer 94 (2002) 786–792.
[72] Y. Mishima, E. Nagasaki, Y. Terui, T. Irie, S. Takahashi, Y. Ito, M. Oguchi, K. Kawabata, S. Kamata, K. Hatake, Combination chemotherapy (cyclophosphamide, doxorubicin, and vincristine with continuous-infusion cisplatin and etoposide) and radiotherapy with stem cell support can be beneficial for adolescents and adults with estheisoneuroblastoma, Cancer 101 (2004) 1437–1444.
[73] D. Bhatia, S. Surana, S. Chakraborty, S.P. Koushika, Y. Krishnan, A synthetic icosahedral DNA-based host–cargo complex for functional in vivo imaging, Nat. Commun. 2 (2011) 339.
[74] J.A. Thomas, R.N. Buchsbaum, A. Zimniak, E. Racker, Intracellular pH measurements in ehrlich ascites tumor-cells utilizing spectroscopic probes generated insitu, Biochemistry 18 (1979) 2210–2218.
[75] G.R. Martin, R.K. Jain, Noninvasive measurement of interstitial pH profiles in normal and neoplastic tissue using fluorescence ratio imaging microscopy, Cancer Res. 54 (1994) 5670–5674.
[76] Y.G. Ke, L.L. Ong, W.M. Shih, P. Yin, Three-dimensional structures self-assembled from DNA bricks, Science 338 (2012) 1177–1183.
[77] Q.A. Mei, X.X. Wei, F.Y. Su, Y. Liu, C. Youngbull, R. Johnson, S. Lindsay, H. Yan, D. Meldrum, Stability of DNA origami nanoarrays in cell lysate, Nano Lett. 11 (2011) 1477–1482.
[78] M.C. Palanca-Wessels, M.T. Barrett, P.C. Galipeau, K.L. Rohrer, B.J. Reid, P.S. Rabinovitch, Genetic analysis of long-term Barrett's esophagus epithelial cultures exhibiting cytogenetic and ploidy abnormalities, Gastroenterology 114 (1998) 295–304.
[79] Y.X. Zhao, A. Shaw, X. Zeng, E. Benson, A.M. Nystrom, B. Hogberg, DNA origami delivery system for cancer therapy with tunable release properties, ACS Nano 6 (2012) 8684–8691.
[80] H. Dietz, S.M. Douglas, W.M. Shih, Folding DNA into twisted and curved nanoscale shapes, Science 325 (2009) 725–730.
[81] Q. Jiang, C. Song, J. Nangreave, X. Liu, L. Lin, D. Qiu, Z.G. Wang, G. Zou, X. Liang, H. Yan, B. Ding, DNA origami as a carrier for circumvention of drug resistance, J. Am. Chem. Soc. 134 (2012) 13396–13403.
[82] I. Pastan, M.M. Gottesman, Multidrug resistance, Annu. Rev. Med. 42 (1991) 277–286.
[83] M.M. Gottesman, Mechanisms of cancer drug resistance, Annu. Rev. Med. 53 (2002) 615–627.
[84] M. Schindler, S. Grabski, E. Hoff, S.M. Simon, Defective pH regulation of acidic compartments in human breast cancer cells (MCF-7) is normalized in adriamycin-resistant cells (MCF-7adr), Biochemistry 35 (1996) 2811–2817.
[85] J.Z. Fuks, S. Wadler, P.H. Wiernik, Phase-I and phase-II agents in cancer-therapy — 2 cisplatin analogs and high-dose cisplatin in hypertonic saline or with thiosulfate protection, J. Clin. Pharmacol. 27 (1987) 357–365.
[86] N. Altan, Y. Chen, M. Schindler, S.M. Simon, Tamoxifen inhibits acidification in cells independent of the estrogen receptor, Proc. Natl. Acad. Sci. U. S. A. 96 (1999) 4432–4437.
[87] S.J. Hurwitz, M. Terashima, N. Mizunuma, C.A. Slapak, Vesicular anthracycline accumulation in doxorubicin-selected U-937 cells: participation of lysosomes, Blood 89 (1997) 3745–3754.
[88] S.M. Douglas, I. Bachelet, G.M. Church, A logic-gated nanorobot for targeted transport of molecular payloads, Science 335 (2012) 831–834.
[89] S. Beyer, P. Nickels, F.C. Simmel, Periodic DNA nanotemplates synthesized by rolling circle amplification, Nano Lett. 5 (2005) 719–722.
[90] Z.X. Deng, Y. Tian, S.H. Lee, A.E. Ribbe, C.D. Mao, DNA-encoded self-assembly of gold nanoparticles into one-dimensional arrays, Angew. Chem. Int. Ed. 44 (2005) 3582–3585.
[91] G.D. Hamblin, K.M. Carneiro, J.F. Fakhoury, K.E. Bujold, H.F. Sleiman, Rolling circle amplification-templated DNA nanotubes show increased stability and cell penetration ability, J. Am. Chem. Soc. 134 (2012) 2888–2891.
[92] P.K. Lo, P. Karam, F.A. Aldaye, C.K. McLaughlin, G.D. Hamblin, G. Cosa, H.F. Sleiman, Loading and selective release of cargo in DNA nanotubes with longitudinal variation, Nat. Chem. 2 (2010) 319–328.
[93] H.P. Liu, Y. Chen, Y. He, A.E. Ribbe, C.D. Mao, Approaching the limit: can one DNA oligonucleotide assemble into large nanostructures? Angew. Chem. Int. Ed. 45 (2006) 1942–1945.
[94] D.A. Giljohann, D.S. Seferos, L.D. Weston, M.D. Massich, P.C. Patel, C.A. Mirkin, Gold nanoparticles for biology and medicine, Angew. Chem. Int. Ed. 49 (2010) 3280–3294.
[95] J.S. Lee, A.K.R. Lytton-Jean, S.J. Hurst, C.A. Mirkin, Silver nanoparticle-oligonucleotide conjugates based on DNA with triple cyclic disulfide moieties, Nano Lett. 7 (2007) 2112–2115.
[96] J.I. Cutler, D. Zheng, X.Y. Xu, D.A. Giljohann, C.A. Mirkin, Polyvalent oligonucleotide iron oxide nanoparticle "click" conjugates, Nano Lett. 10 (2010) 1477–1480.
[97] G.P. Mitchell, C.A. Mirkin, R.L. Letsinger, Programmed assembly of DNA functionalized quantum dots, J. Am. Chem. Soc. 121 (1999) 8122–8123.
[98] M. Kwak, A. Herrmann, Nucleic acid/organic polymer hybrid materials: synthesis, superstructures, and applications, Angew. Chem. Int. Ed. 49 (2010) 8574–8587.
[99] F.E. Alemdaroglu, A. Herrmann, DNA meets synthetic polymers-highly versatile hybrid materials, Org. Biomol. Chem. 5 (2007) 1311.
[100] M. Kwak, A. Herrmann, Nucleic acid amphiphiles: synthesis and self-assembled nanostructures, Chem. Soc. Rev. 40 (2011) 5745–5755.
[101] R. Elghanian, J.J. Storhoff, R.C. Mucic, R.L. Letsinger, C.A. Mirkin, Selective colorimetric detection of polynucleotides based on the distance-dependent optical properties of gold nanoparticles, Science 277 (1997) 1078–1081.
[102] J.S. Lee, D.S. Seferos, D.A. Giljohann, C.A. Mirkin, Thermodynamically controlled separation of polyvalent 2-nm gold nanoparticle-oligonucleotide conjugates, J. Am. Chem. Soc. 130 (2008) 5430–5431.
[103] S.J. Hurst, A.K.R. Lytton-Jean, C.A. Mirkin, Maximizing DNA loading on a range of gold nanoparticle sizes, Anal. Chem. 78 (2006) 8313–8318.
[104] G. Bhabra, A. Sood, B. Fisher, L. Cartwright, M. Saunders, W.H. Evans, A. Surprenant, G. Lopez-Castejon, S. Mann, S.A. Davis, L.A. Hails, E. Ingham, P. Verkade, J. Lane, K. Heesom, R. Newson, C.P. Case, Nanoparticles can cause DNA damage across a cellular barrier, Nat. Nanotechnol. 4 (2009) 876–883.
[105] A. Nel, T. Xia, L. Madler, N. Li, Toxic potential of materials at the nanolevel, Science 311 (2006) 622–627.
[106] Y. Pan, S. Neuss, A. Leifert, M. Fischler, F. Wen, U. Simon, G. Schmid, W. Brandau, W. Jahnen-Dechent, Size-dependent cytotoxicity of gold nanoparticles, Small 3 (2007) 1941–1949.
[107] J.I. Cutler, K. Zhang, D. Zheng, E. Auyeung, A.E. Prigodich, C.A. Mirkin, Polyvalent nucleic acid nanostructures, J. Am. Chem. Soc. 133 (2011) 9254–9257.
[108] D.S. Seferos, A.E. Prigodich, D.A. Giljohann, P.C. Patel, C.A. Mirkin, Polyvalent DNA nanoparticle conjugates stabilize nucleic acids, Nano Lett. 9 (2009) 308–311.
[109] J.P. Behr, Synthetic gene-transfer vectors, Acc. Chem. Res. 26 (1993) 274–278.
[110] D. Luo, W.M. Saltzman, Synthetic DNA delivery systems, Nat. Biotechnol. 18 (2000) 33–37.
[111] D.A. Giljohann, D.S. Seferos, P.C. Patel, J.E. Millstone, N.L. Rosi, C.A. Mirkin, Oligonucleotide loading determines cellular uptake of DNA-modified gold nanoparticles, Nano Lett. 7 (2007) 3818–3821.
[112] B.D. Chithrani, A.A. Ghazani, W.C.W. Chan, Determining the size and shape dependence of gold nanoparticle uptake into mammalian cells, Nano Lett. 6 (2006) 662–668.
[113] A. Matsumoto, M. Naito, H. Itakura, S. Ikemoto, H. Asaoka, I. Hayakawa, H. Kanamori, H. Aburatani, F. Takaku, H. Suzuki, Y. Kobari, T. Miyai, K. Takahashi, E.H. Cohen, R. Wydro, D.E. Housman, T. Kodama, Human macrophage scavenger receptors — primary structure, expression, and localization in atherosclerotic lesions, Proc. Natl. Acad. Sci. U. S. A. 87 (1990) 9133–9137.
[114] D.R. Greaves, S. Gordon, Recent insights into the biology of macrophage scavenger receptors, J. Lipid Res. 46 (2005) 11–20.
[115] M.K. Bijsterbosch, M. Manoharan, E.T. Rump, R.L.A. DeVrueh, R. vanVeghel, K.L. Tivel, E.A.L. Biessen, C.F. Bennett, P.D. Cook, T.J.C. vanBerkel, In vivo fate of phosphorothioate antisense oligodeoxynucleotides: predominant uptake by scavenger receptors on endothelial liver cells, Nucleic Acids Res. 25 (1997) 3290–3296.
[116] N. Liu, M. Hentschel, T. Weiss, A.P. Alivisatos, H. Giessen, Three-dimensional plasmon rulers, Science 332 (2011) 1407–1410.
[117] K. Zhang, L.L. Hao, S.J. Hurst, C.A. Mirkin, Antibody-linked spherical nucleic acids for cellular targeting, J. Am. Chem. Soc. 134 (2012) 16488–16491.
[118] N.E. Hynes, H.A. Lane, ERBB receptors and cancer: the complexity of targeted inhibitors, Nat. Rev. Cancer 5 (2005) 341–354.
[119] J. Baselga, S.M. Swain, Novel anticancer targets: revisiting ERBB2 and discovering ERBB3, Nat. Rev. Cancer 9 (2009) 463–475.
[120] S. Dhar, W.L. Daniel, D.A. Giljohann, C.A. Mirkin, S.J. Lippard, Polyvalent oligonucleotide gold nanoparticle conjugates as delivery vehicles for platinum(IV) warheads, J. Am. Chem. Soc. 131 (2009) 14652–14653.
[121] E.R. Jamieson, S.J. Lippard, Structure, recognition, and processing of cisplatin-DNA adducts, Chem. Rev. 99 (1999) 2467–2498.
[122] B. Rosenber, L. Vancamp, J.E. Trosko, V.H. Mansour, Platinum compounds — a new class of potent antitumour agents, Nature 222 (1969) 385–386.
[123] X.Q. Zhang, X. Xu, R. Lam, D. Giljohann, D. Ho, C.A. Mirkin, Strategy for increasing drug solubility and efficacy through covalent attachment to polyvalent DNA–nanoparticle conjugates, ACS Nano 5 (2011) 6962–6970.
[124] C.M. Alexander, J.C. Dabrowiak, M.M. Maye, Investigation of the drug binding properties and cytotoxicity of DNA-capped nanoparticles designed as delivery vehicles for the anticancer agents doxorubicin and actinomycin D, Bioconjug. Chem. 23 (2012) 2061–2070.
[125] J.B. Chaires, J.E. Herrera, M.J. Waring, Preferential binding of daunomycin to 5′ ATCG and 5′ATGC sequences revealed by footprinting titration experiments, Biochemistry 29 (1990) 6145–6153.

[126] F. Sha, F.M. Chen, Actinomycin D binds strongly to d(CGACGACG) and d(CGTCGTCG), Biophys. J. 79 (2000) 2095–2104.
[127] D. Kim, Y.Y. Jeong, S. Jon, A drug-loaded aptamer-gold nanoparticle bioconjugate for combined CT imaging and therapy of prostate cancer, ACS Nano 4 (2010) 3689–3696.
[128] V. Bagalkot, O.C. Farokhzad, R. Langer, S. Jon, An aptamer–doxorubicin physical conjugate as a novel targeted drug-delivery platform, Angew. Chem. Int. Ed. 45 (2006) 8149–8152.
[129] Z. Xiao, C. Ji, J. Shi, E.M. Pridgen, J. Frieder, J. Wu, O.C. Farokhzad, DNA self-assembly of targeted near-infrared-responsive gold nanoparticles for cancer thermo-chemotherapy, Angew. Chem. Int. Ed. 51 (2012) 11853–11857.
[130] V. Ntziachristos, J. Ripoll, L.H.V. Wang, R. Weissleder, Looking and listening to light: the evolution of whole-body photonic imaging, Nat. Biotechnol. 23 (2005) 313–320.
[131] M. Wei, N. Chen, J. Li, M. Yin, L. Liang, Y. He, H.Y. Song, C.H. Fan, Q. Huang, Polyvalent immunostimulatory nanoagents with self-assembled CpG oligonucleotide-conjugated gold nanoparticles, Angew. Chem. Int. Ed. 51 (2012) 1202–1206.
[132] B.G. Trewyn, J.A. Nieweg, Y. Zhao, V.S.Y. Lin, Biocompatible mesoporous silica nanoparticles with different morphologies for animal cell membrane, penetration, Chem. Eng. J. 137 (2008) 23–29.
[133] J. Kecht, A. Schlossbauer, T. Bein, Selective functionalization of the outer and inner surfaces in mesoporous silica nanoparticles, Chem. Mater. 20 (2008) 7207–7214.
[134] V. Cauda, A. Schlossbauer, J. Kecht, A. Zurner, T. Bein, Multiple core–shell functionalized colloidal mesoporous silica nanoparticles, J. Am. Chem. Soc. 131 (2009) 11361–11370.
[135] E. Climent, A. Bernardos, R. Martinez-Manez, A. Maquieira, M.D. Marcos, N. Pastor-Navarro, R. Puchades, F. Sancenon, J. Soto, P. Amoros, Controlled delivery systems using antibody-capped mesoporous nanocontainers, J. Am. Chem. Soc. 131 (2009) 14075–14080.
[136] K. Patel, S. Angelos, W.R. Dichtel, A. Coskun, Y.W. Yang, J.I. Zink, J.F. Stoddart, Enzyme-responsive snap-top covered silica nanocontainers, J. Am. Chem. Soc. 130 (2008) 2382–2383.
[137] T.D. Nguyen, H.R. Tseng, P.C. Celestre, A.H. Flood, Y. Liu, J.F. Stoddart, J.I. Zink, A reversible molecular valve, Proc. Natl. Acad. Sci. U. S. A. 102 (2005) 10029–10034.
[138] C.B. Gao, H.Q. Zheng, L. Xing, M.H. Shu, S.N. Che, Designable coordination bonding in mesopores as a pH-responsive release system, Chem. Mater. 22 (2010) 5437–5444.
[139] N.G. Liu, D.R. Dunphy, P. Atanassov, S.D. Bunge, Z. Chen, G.P. Lopez, T.J. Boyle, C.J. Brinker, Photoregulation of mass transport through a photoresponsive azobenzene-modified nanoporous membrane, Nano Lett. 4 (2004) 551–554.
[140] C.E. Chen, J. Geng, F. Pu, X.J. Yang, J.S. Ren, X.G. Qu, Polyvalent nucleic acid/mesoporous silica nanoparticle conjugates: dual stimuli-responsive vehicles for intracellular drug delivery, Angew. Chem. Int. Ed. 50 (2011) 882–886.
[141] Q. Yuan, Y. Zhang, T. Chen, D. Lu, Z. Zhao, X. Zhang, Z. Li, C.H. Yan, W. Tan, Photon-manipulated drug release from a mesoporous nanocontainer controlled by azobenzene-modified nucleic acid, ACS Nano 6 (2012) 6337–6344.
[142] C. Chen, F. Pu, Z. Huang, Z. Liu, J. Ren, X. Qu, Stimuli-responsive controlled-release system using quadruplex DNA-capped silica nanocontainers, Nucleic Acids Res. 39 (2011) 1638–1644.
[143] K. Gehring, J.L. Leroy, M. Gueron, A tetrameric DNA-structure with protonated cytosine. Cytosine base-pairs, Nature 363 (1993) 561–565.
[144] M. Gueron, J.L. Leroy, The i-motif in nucleic acids, Curr. Opin. Struct. Biol. 10 (2000) 326–331.
[145] D.G. He, X.X. He, K.M. Wang, J. Cao, Y.X. Zhao, A photon-fueled gate-like delivery system using i-motif DNA functionalized mesoporous silica nanoparticles, Adv. Funct. Mater. 22 (2012) 4704–4710.
[146] Z. Zhang, D. Balogh, F. Wang, I. Willner, Smart mesoporous SiO_2 nanoparticles for the DNAzyme-induced multiplexed release of substrates, J. Am. Chem. Soc. 135 (2013) 1934–1940.
[147] A. Schlossbauer, S. Warncke, P.M.E. Gramlich, J. Kecht, A. Manetto, T. Carell, T. Bein, A programmable DNA-based molecular valve for colloidal mesoporous silica, Angew. Chem. Int. Ed. 49 (2010) 4734–4737.
[148] E. Ruiz-Hernandez, A. Baeza, M. Vallet-Regi, Smart drug delivery through DNA/magnetic nanoparticle gates, ACS Nano 5 (2011) 1259–1266.
[149] A. Rosler, G.W.M. Vandermeulen, H.A. Klok, Advanced drug delivery devices via self-assembly of amphiphilic block copolymers, Adv. Drug Deliv. Rev. 64 (2012) 270–279.
[150] M. Moffitt, K. Khougaz, A. Eisenberg, Micellization of ionic block copolymers, Acc. Chem. Res. 29 (1996) 95–102.
[151] F.M. Veronese, G. Pasut, PEGylation, successful approach to drug delivery, Drug Discov. Today 10 (2005) 1451–1458.
[152] M.H. Caruthers, Chemical synthesis of DNA and DNA analogs, Acc. Chem. Res. 24 (1991) 278–284.
[153] F.E. Alemdaroglu, W. Zhuang, L. Zophel, J. Wang, R. Berger, J.P. Rabe, A. Herrmann, Generation of multiblock copolymers by PCR: synthesis, visualization and nanomechanical properties, Nano Lett. 9 (2009) 3658–3662.
[154] M.S. Ayaz, M. Kwak, F.E. Alemdaroglu, J. Wang, R. Berger, A. Herrmann, Synthesis of DNA block copolymers with extended nucleic acid segments by enzymatic ligation: cut and paste large hybrid architectures, Chem. Commun. 47 (2011) 2243–2245.
[155] F.E. Alemdaroglu, J. Wang, M. Borsch, R. Berger, A. Herrmann, Enzymatic control of the size of DNA block copolymer nanoparticles, Angew. Chem. Int. Ed. 47 (2008) 974–976.
[156] K. Ding, F.E. Alemdaroglu, M. Boersch, R. Berger, A. Herrmann, Engineering the structural properties of DNA block copolymer micelles by molecular recogntition, Angew. Chem. Int. Ed. 46 (2007) 1172–1175.
[157] F.E. Alemdaroglu, N.C. Alemdaroglu, P. Langguth, A. Herrmann, Cellular uptake of DNA block copolymer micelles with different shapes, Macromol. Rapid. Commun. 29 (2008) 326–329.
[158] F.E. Alemdaroglu, N.C. Alemdaroglu, P. Langguth, A. Herrmann, DNA block copolymer micelles — a combinatorial tool for cancer nanotechnology, Adv. Mater. 20 (2008) 899–902.
[159] Y. Wu, K. Sefah, H. Liu, R. Wang, W. Tan, From the cover: DNA aptamer-micelle as an efficient detection/delivery vehicle toward cancer cells, Proc. Natl. Acad. Sci. U. S. A. 107 (2009) 5–10.
[160] M. Kwak, A.J. Musser, J. Lee, A. Herrmann, DNA-functionalised blend micelles: mix and fix polymeric hybrid nanostructures, Chem. Commun. 46 (2010) 4935.
[161] M. Kwak, I.J. Minten, D.-M. Anaya, A.J. Musser, M. Brasch, R.J.M. Nolte, K. Mullen, J.J.L.M. Cornelissen, A. Herrmann, Virus-like particles templated by DNA micelles: a general method for loading virus nanocarriers, J. Am. Chem. Soc. 132 (2010) 7834–7835.
[162] A. Rodriguez-Pulido, A.I. Kondrachuk, D.K. Prusty, J. Gao, M.A. Loi, A. Herrmann, Light-triggered sequence-specific cargo release from DNA block copolymer-lipid vesicles, Angew. Chem. Int. Ed. 52 (2013) 1008–1012.
[163] Z. Cao, R. Tong, A. Mishra, W. Xu, G.C. Wong, J. Cheng, Y. Lu, Reversible cell-specific drug delivery with aptamer-functionalized liposomes, Angew. Chem. Int. Ed. 48 (2009) 6494–6498.
[164] C.K. McLaughlin, G.D. Hamblin, K.D. Hanni, J.W. Conway, M.K. Nayak, K.M. Carneiro, H.S. Bazzi, H.F. Sleiman, Three-dimensional organization of block copolymers on “DNA-minimal” scaffolds, J. Am. Chem. Soc. 134 (2012) 4280–4286.